Interactions in inorganic molecular crystals. Electronic spectra of ReF$_6$ pure and mixed crystals

E. R. Bernstein and G. R. Meredith

Interactions in inorganic molecular crystals. Electronic spectra of ReF$_6$ pure and mixed crystals*†

E. R. Bernstein‡ and G. R. Meredith‡

Department of Chemistry, Princeton University, Princeton, New Jersey 08540
(Received 15 August 1975)

Electronic absorption spectra of ReF$_6$($5d^1$) are obtained for the pure crystal and UF$_6$, MoF$_6$, and WF$_6$ mixed crystals. The observed transition arises from an intraconfigurational $t_{2g} \rightarrow t_{2g}$ promotion characterized $\Gamma_{7g} \leftarrow \Gamma_{8g}$ in 0_h symmetry. The pure crystal is predicted to undergo a magnetic phase transition below ~ 1.5 K. Pair spectra, two-molecule transitions, the ground state Jahn–Teller effect, linewidths, and vibrational assignments are discussed. The major mechanism for pair coupling and magnetic ordering is identified as superexchange through low lying delocalized charge transfer bands. These interactions are qualitatively discussed and energy localizing and delocalizing interactions are separated.

I. INTRODUCTION

Since the initial study of the electronic structure of transition metal hexafluorides some 15 years ago,[1] there has been considerable interest in the vibrational,[2] electronic,[3] and magnetic[4] properties of these systems. Theoretical studies dealing with molecular orbital[5] and crystal field[6] descriptions of molecular species XF$_6$(X = 3d, 4d, 5d, and 5f metal ions in a formal valence state of plus six) have also appeared. This previous work notwithstanding, it seems fair to say that only the most rudimentary understanding of electronic distributions for octahedral inorganic molecules at present exists. The electronic structure problem is compounded by the presence of supposedly large vibronic interactions (the Jahn–Teller effect)[2,7] in either the ground (ReF$_6$, OsF$_6$, TcF$_6$, RuF$_6$) or excited electronic states of the 0_h zero-order structure. The homologous transition metal hexafluoride series affords a system for further and more detailed investigations into the interaction between electronic and vibrational degrees of freedom in molecules.[8,9] In addition, high atomic weight metal ions do not often form discrete molecular entities and such systems have unusual structural, chemical, and bonding properties. Detailed spectroscopic studies of these systems can, at least in principle, aid in the elucidation of such points as what orbitals are involved in bonding, what is the electron density in bonding molecular orbitals, and what is the extent of delocalization of unpaired electrons over the molecular frame work.

Transition metal hexafluoride molecules are thermodynamically stable,[10] have vapor pressures in excess of 100 torr at 300 K, and form low melting molecular solids. As such, they are also a general series available for the study of molecular crystals. In addition to high free molecule symmetry and the availability of a complete series of molecules with systematic properties, the hexafluorides are simple (have relatively few atoms) and have many accessible electronic states. This is to be contrasted with the most heavily studied molecular crystals, the aromatic organics, for which usually only one singlet and one triplet state are available for detailed study.[11] The presence of unpaired electrons makes it possible to observe magnetic resonance spectra in many, if not all, of the low lying d or f excited electronic states.[12]

A number of important advances in understanding molecular solids have come through the study of isotropic mixed crystals (the ideal mixed crystal limit),[11] and it turns out, as we shall demonstrate, the concept of the ideal mixed crystal is even more faithfully reproduced for the closed shell host systems of WF$_6$, MoF$_6$, and UF$_6$ with 0.1% to 1.0% paramagnetic guest species, than for the original source of this concept. Using the XF$_6$ species, it is possible to study in depth a totally different molecular solid, thereby checking the applicability of previous theory and the generality of various approximations. On the other hand, owing to the high atomic weight of the central ion and the presence of unpaired electrons, large spin orbit coupling and exchange interactions are expected in these systems. It therefore becomes necessary to incorporate a number of typically "ionic crystal concepts" into molecular crystal theory.

This paper deals specifically with the electronic spectra of ReF$_6$ ($5d^1$) pure and mixed crystals. From these data we will present information concerning both molecular properties (Jahn–Teller and vibronic interaction) and intermolecular interactions. ReF$_6$ was chosen as the first in this series to be studied because of its simple electronic structure and well isolated d–d transition in the near infrared (2.0 μm). The optical data presented below support six main conclusions concerning XF$_6$ crystals: (1) electron exchange interactions are more important than excitation exchange (exciton) interactions in the pure crystal—ReF$_6$ is expected to magnetically order at temperatures less than 1.5 K; (2) the electron exchange mechanism is superexchange and is inextricably associated with low lying charge transfer bands in pure and mixed crystals; (3) exciton and exchange interactions can, in part, be separated by studying pair spectra in various host–guest systems with both high and low energy delocalized charge transfer bands and comparing them to pure crystal features; (4) two-molecule or two-particle transitions are observed and positively identified, in which one molecule is electronically excited and one molecule is vibrationally excited—such effects are shown to be responsible for much of the so-called vibronic intensity; (5) theoretically expected linewidths are observed; and (6) the observed spectra are definitely those which are characteristic of a molecule, and many conclusions

TABLE I. Physical properties of some transition metal hexafluorides.

Molecule	Metal–fluorine distance (Å)	Vapor pressure at 300 K (torr)	Solid transition T(°C)	ΔS(eu)	Fusion T(°C)	ΔS(eu)	Vaporization T(°C)	ΔS(eu)
ReF$_6$	1.832[a]	590[b]	−3.45	7.52[b]	18.5	3.80[b]	18.5	23.5[b]
MoF$_6$	1.820[c]	584[d]	−9.67	7.41[e]	17.58	3.56[e]	25	22.2[e]
WF$_6$	1.833[f]	1008[d]	−8.5	7.81[h]	2.0	3.56[h]	...	21.8[d]
UF$_6$	1.996[f]	127[g]	...	...	64.05	13.61[f]	64.05	20.2[f]

[a]E. J. Jacob and L. S. Bartell, J. Chem. Phys. 53, 2231 (1970).
[b]J. G. Malm and H. Selig, J. Inorg. Nucl. Chem. 20, 189 (1961).
[c]H. Seip, Sel. Top. Struct. Chem. 1967, 26.
[d]G. H. Cady and G. B. Hargreaves, J. Chem. Soc. London. 1961, 1563.
[e]D. W. Osborne, L. Shreiva, J. G. Malm, H. Selig, and L. Rochester, J. Chem. Phys. 44, 2802 (1966).
[f]B. Weinstock, Rec. Chem. Prog. 23, 23 (1962).
[g]G. D. Oliver, H. F. Milton, and J. W. Grysard, J. Am. Chem. Soc. 75, 2827 (1953).
[h]E. F. Westrum, Jr., J. Chim. Phys. 63, 47 (1966).

concerning the molecule (Jahn–Teller effect, vibronic coupling, electronic distribution) are possible using molecular crystal data.

The remainder of the paper is divided as follows. Sec. II gives a review of the general physical, electronic, magnetic, and vibrational properties of ReF$_6$ as well as its crystal structure. In Sec. III a theoretical description of molecular and crystalline ReF$_6$ is presented and the Hamiltonian appropriate for inorganic molecular mixed ("isotopic") and pure crystals is given. Sections IV and V present experimental procedures and results. The results are discussed in Sec. VI, and finally conclusions and a few comments about future investigations and other systems are made in Sec. VII.

II. PROPERTIES OF ReF$_6$ MOLECULE AND CRYSTAL

A. General

ReF$_6$ is paramagnetic and can be thought of as a molecule with one unpaired 5d metal electron. Its thermodynamic properties, as well as melting point, boiling point, vapor pressure, and bond distances have been studied over a wide range of variables. Table I contains a summary of some of the more useful ones for our purposes. Properties of other hexafluorides used in this work (UF$_6$, WF$_6$, MoF$_6$) will also be found in Table I for comparison. It is quite obvious from these data that the general XF$_6$ species is molecular in nature and that these molecules form weakly bound molecular solids.

B. Electronic

The major insight into the spectroscopic properties of transition metal hexafluorides stems from the original work of Moffitt, Goodman, Fred, and Weinstock.[1] The basic free molecule model is that of 4d or 5d electrons in a strong octahedral crystal field (10$Dq \sim$ 30 000 cm^{-1} for ReF$_6$) further perturbed by large spin–orbit coupling ($\xi \sim$ 3050 cm^{-1} for ReF$_6$) and, when appropriate, a substantial electron–electron repulsion term ($G \sim$ 2500 cm^{-1} IrF$_6$, (5d)^3). The near infrared and visible region of the spectrum can then be assumed to arise from intraconfigurational transitions between states

of a spin–orbit, electron–electron repulsion split $(dt_{2g})^n$ configuration. The separations between states of the $(dt_{2g})^n$ configuration have been shown, using the Wigner–Eckhart theorem, to be formally equivalent to those of the p^{6-n} atomic configuration.[1] The sharp-line optical spectra can then be modeled by three parameters.

"Crystal field" interconfigurational transitions $[(dt_{2g})^n \to (dt_{2g})^{n-1}e_g]$ lie at roughly 30 000 cm^{-1} for the 5d series and overlap the fluorine-to-metal charge transfer systems.[1,3] Little is known about the nature of these states.

The charge transfer transitions, believed to be of the ligand-to-metal variety, have also been studied, in both the paramagnetic (ReF$_6$) and closed shell (MoF$_6$, WF$_6$, UF$_6$) systems.[1,3f] The general conclusion from these studies favors transitions associated with a ligand π- or σ-orbital electron going to a metal $(dt_{2g})^n$ orbital. This would be consistent with roughly 25 000 cm^{-1} difference in charge transfer transition energy between ReF$_6$ and Mo, WF$_6$.

C. Vibrations

The normal modes of a seven atom molecule with O_h symmetry are well known.[2,13] Considering the relative simplicity of this molecule it is surprising that a number of problems still remain with the vibrational frequencies in ReF$_6$. Some of these will be touched on in this report: $\nu_1 - \nu_3$ assignment in the solid, ν_6 energy, and the Jahn–Teller nature of ν_2 and ν_5. The difficulties with the previous gas phase vibrational spectra of this series have been poor spectral resolution ($\sim$ 5–10 cm^{-1}) and combination, overtone, hot band, and rotational congestion of the spectra.

D. Magnetic susceptibility

The magnetic susceptibility of ReF$_6$ has been previously measured in the temperature range 14–300 K[4b] and a magnetic moment per molecule of 0.25 Bohr magneton was found. This yields an effective spectroscopic splitting factor (g) of about 0.3. We have repeated these measurements and extended them to 4.2 and 1.5 K. Results will be presented in Secs. V

and VI but are in substantial agreement with those of Ref. 4(b) for the temperature ranges that overlap in the two studies. The magnetic moment per molecule (0_h) and the susceptibility can be qualitatively accounted for by the first-order theoretical model discussed above with only minor elaboration.

E. Crystal structure

The crystal structure of UF_6 was first determined by Hoard and Stroupe by single crystal x-ray diffraction techniques at 300 K.[14a] This early study found the space group to be D_{2h}^{16}-$Pnma$-with four molecules per primitive unit cell at sites of $C_s(m)$ symmetry. The uranium atoms and two fluorine atoms (F_1 and F_2) are contained in the site plane. These "axial" fluorines are at a distance of 2.12 Å from the central uranium, while the four other "planar" fluorines (F_3, F_3', F_4, F_4') lie off the site plane and are related in pairs by it. Even though it is not a symmetry constraint of the structure, the four planar fluorines are, within experimental error, equidistant from the central uranium atom at 2.01 Å. The molecule in the site thus looks much like a distorted octahedron (D_{4h}), with one of its fourfold axes elongated. This approximate D_{4h} symmetry is supported by ^{19}F NMR studies.[15] The z axis (long axis on which the axial fluorines approximately lie) makes an angle of about 35° with the crystallographic c direction. The four molecules in the unit cell can be related to one another by the twofold screw axes (interchange operations), such that: $C_2^b I = II$, $C_2^b I = III$, and $C_2^c I = IV$. The coordinate systems at each site are thus righthanded and properly phased with respect to each other. The interchange group is isomorphic to the point group D_2, the factor group is isomorphic to the point group D_{2h}, and the site group is C_s.

The other hexafluorides have a body-centered cubic crystal structure near their melting points and undergo phase transitions to the UF_6 structure below ~0 °C.[14b] Atomic positions for hexafluorides other than uranium have not been determined by x-ray diffraction. The unit cell parameters are given in Table II for each structure.

Recently, three powder neutron diffraction studies of transition metal hexafluorides have appeared, one dealing with UF_6 and the other two dealing with cubic and orthorhombic MoF_6.[14c] These studies in general confirm the previous work but give UF_6 more C_s dis-

TABLE II. Unit cell parameters based on $Pnma$.

Molecule	Temperature (°C)	a (Å)	b (Å)	c (Å)
ReF_6[a]	−22	9.61	8.76	5.06
MoF_6	−36[a]	9.61	8.75	5.07
	−80[b]	9.559	8.668	5.015
WF_6[a]	−20	9.68	8.81	5.09
UF_6	+25[c]	9.90	8.96	5.21
	−25[d]	9.80	8.86	5.15

[a]Reference 14(b).
[b]Reference 14(c).
[c]Reference 14(a).
[d]Temperature adjusted—see text.

TABLE III. Crystal distances between atoms of neighboring UF_6 molecules.[a]

Pair	M—M distance (Å)	Degeneracy	Range of F—F distances (Å)
I–II	5.254	2	3.046–8.654
	6.032	2	3.035–9.591
	8.546	2	5.256–12.132
I–III	5.231	2	3.079–8.814
	6.760	2	3.104–10.668
	7.954	2	3.183–11.652
	8.637	2	5.368–12.353
I–IV	5.705	4	3.030–9.200
I–I$_C'$	5.207	2	2.960–9.018
I–I$_B'$	8.962	2	6.148–12.123

[a]Calculated from parameters in Ref. 14(a).

torted than Hoard and Stroupe's D_{4h} model [U–F_1 = 1.96 Å; U–F_2 = 2.28 Å; U–F_3 ~ U–F_4 ~ 1.90 Å]. MoF_6, on the other hand, is close to symmetric with Mo–F_i ~ 1.82 ± (0.02) Å. Unit cell parameters for MoF_6 determined by neutron powder diffraction at 193 K are found in Table II. Interestingly enough, the F–F intra- and interlayer contacts are roughly the same in both structures 3.10 ± 0.02 Å. The metal–metal contacts in UF_6 are much longer (by 0.2 and 0.4 Å) than in MoF_6, however, owing to the asymmetrical position of the uranium atoms. Therefore, if metal–metal interactions were central to the variation of intermolecular interactions among different hosts discussed later, one would expect that larger interactions would be found for ReF_6 in MoF_6 and WF_6 rather than for ReF_6 in UF_6. Since the large interactions are found for ReF_6 pure and ReF_6/UF_6 mixed crystals (vide infra), metal–metal and fluorine–fluorine contacts must not be of central importance for the electronic interactions observed in the spectra.

It is unfortunate that all the data were not collected at the same temperature. Using a rough number of 2×10^{-4} for the linear thermal expansion coefficient $\alpha[= (1/3V)(\partial V/\partial T)_p]$ the change in unit cell parameters is roughly 2% over a 100 K temperature range. The values of unit cell parameters for UF_6 become a(250 K) = 9.80 Å, b(250 K) = 8.86 Å, and c(250 K) = 5.15 Å, and a(190 K) = 9.69 Å, b(190 K) = 8.75 Å, and c(190 K) = 5.09 Å. Such considerations certainly make the value of the unit cell parameters for the 4d and 5d systems identical. The UF_6 axes are apparently somewhat longer than those of the 4d and 5d series hexafluorides.

It is interesting to consider the location and number of near neighbors for this structure. These data are presented in Table III. Because of the short c axis, the nearest neighbors related by a translation along the c axis are expected to have the greatest pair-wise interaction in this structure. The fluorine–fluorine nearest contacts also bear this out (see Table III). It should be noted that there are twice as many I–IV equivalent contacts as there are I–II and I–III equivalent contacts. This arises because the site mirror is parallel to C_2^c and thus generates another set of equiva-

lent distances. Only the translationally equivalent con-
tacts in the b- and c directions are short enough for
inclusion in this partial tabulation.

III. THEORY

A. Introduction

The purpose of this section is to present those con-
cepts needed to understand the experimental observa-
tions in inorganic pure and mixed crystals. It will be
necessary to discuss the molecule, various pure and
mixed (host–guest) crystals, excitons, magnetic ex-
change and ordering effects, dimers (pair spectra),
and two-molecule (two-particle) transitions.

Considering the molecular nature of transition metal
hexafluoride solids, it is reasonable to assume a tight
binding limit to partition the crystal Hamiltonian into
sums over site Hamiltonians plus sums over intersite
interaction terms:

$$\mathcal{H}_{cryst} = \sum_{nq} \mathcal{H}_{nq}^{site} + \frac{1}{2} \sum_{n'q' \neq nq} V_{nq,n'q'}$$

$$= \mathcal{H}_{site} + \mathcal{H}' . \tag{III.1}$$

The meaning of these terms is somewhat more complex
than the usual molecular crystal isotopic guest–host
system with which it is useful to draw comparisons.
Since in the isotopic mixed (C_6H_6, C_8H_{10}, etc.) crys-
tals the only difference between the various combina-
tions of mixed and pure crystals is vibrational, the
electronic Hamiltonian remains constant. One would
like to carry over as much of this formalism as pos-
sible to the pure and mixed crystals treated here (ReF_6;
ReF_6/WF_6, MoF_6, UF_6). However, the number of
electrons (both paired and unpaired) changes as the
crystal changes. A site Hamiltonian for a crystal of
closed shell molecules containing one paramagnetic
molecule (at site nq), called the *infinite dilution mixed
crystal*, would then be

$$\mathcal{H}_{nq}^{site} = \mathcal{H}_{nq}^{mol} + (V_{core}^{core})_{nq} + (V_{par}^{core})_{nq} . \tag{III.2}$$

$\mathcal{H}^{mol}$ is the molecular Hamiltonian including the spin-
orbit interaction. The $(V_{core}^{core})_{nq}$ represents the Coulomb
interaction between nuclei and core electrons (closed
shells) at nq and all other cores and their charge bal-
ancing nuclear terms in the crystal. $(V_{par}^{core})_{nq}$ likewise
represents the paramagnetic electrons at nq (with nu-
clear charge compensation) interacting with all cores
and balancing nuclear charge. Using such a definition
we can thus write the Hamiltonians for the various
crystals:

Pure crystal:

$$\mathcal{H}_{pure\ crystal} = \sum_{nq} \mathcal{H}_{nq}^{site} + \frac{1}{2} \sum_{nq \neq n'q'} [(V_{par}^{par})_{nq,n'q'}$$

$$- (V_{core}^{core})_{nq,n'q'}] ; \tag{III.3}$$

Infinite dilution mixed crystal:

$$\mathcal{H}_{IDMC} = \sum_{nq} \mathcal{H}_{nq}^{site} - \frac{1}{2} \sum_{nq \neq n'q'} (V_{core}^{core})_{nq,n'q'} ; \tag{III.4}$$

Dimer or pair in a crystal:

$$\mathcal{H}_{pair} = \sum_{nq} \mathcal{H}_{nq}^{site} + \frac{1}{2} \sum_{nq \neq n'q'} [(V_{par}^{par})_{nq,n'q'} - (V_{core}^{core})_{nq,n'q'}] .$$

$$\tag{III.5}$$

It is of course understood that the appropriate terms
are zero for different site occupancy [i. e., $(V_{par}^{core})_{nq,n'q'}$
$= 0$ if site nq is a closed shell host molecule, etc.]

These definitions yield small $\mathcal{H}'$ by virtue of the
partition which removes monopolar interactions from
intersite terms and the inclusion of interactions with
other site cores in $\mathcal{H}_{nq}^{site}$. However, since we intend
to discuss experimental data, it is the form of the
solution and not the construction of the best partition
that is of concern. The central point is that one can
transfer a specifically constructed site Hamiltonian
(representation) from one crystal system to another.

In a perturbation approach, it is of course most use-
ful to include as much of the crystal interaction as pos-
sible or conceptually convenient in $\mathcal{H}_{site}$, consistent
with the need to transfer $\mathcal{H}_{site}$ between various crystal
systems. For example, this term would include an
effective potential which brings about molecular dis-
tortions and shifts and splittings of molecular energy
levels. The zero-order crystal wavefunctions are sim-
ply antisymmetrized products of the site eigenfunctions.
Perturbation theory is then applied to refine the ener-
gies and wavefunctions. In an even more approximate
treatment, $\mathcal{H}_{nq}^{site} \approx (\mathcal{H}_{mol})_{nq}$ and the usual terms of ex-
citon theory obtain.[11]

An ideal mixed crystal is one for which the host and
guest molecules are identical and the host acts simply
as an isolation matrix for the guest. However, in the
usual isotopic organic systems, which are assumed to
approach this limit rather well, host exciton bands can
cause the guest states to be perturbed by either pseudo-
or real resonance interactions. Hamiltonian complica-
tions notwithstanding, transition metal hexafluorides
may approach the ideal mixed crystal limit much more
closely, as host systems have their first electronic
transitions either in the vacuum (MoF_6 and WF_6) or
near (UF_6) ultraviolet. It should prove useful to char-
acterize ideal mixed crystal systems in the absence
of near resonance interactions; in order to do this,
it is essential to be able to separate, at least in princi-
ple, the various Hamiltonians into transferable site
terms and interaction terms, as has been done above.
Before discussing crystal wavefunctions, it is ap-
propriate to present some properties of ReF_6 molecules
both isolated and in a crystal environment.

B. The molecule in the crystal

The effect of molecular distortion in the low tem-
perature phase of hexafluoride solids is largely de-
scribed by a reduction to D_{4h} symmetry. The Γ_{8g} elec-
tronic levels of the octahedral molecule will split into
Γ_{6g} and Γ_{7g} levels (D_{4h}). The reduction to rigorous C_s
site symmetry cannot remove the remaining Kramers
degeneracy. Figure 1 depicts this situation. The de-
generacies of molecular vibrations will of course be
lifted (see Fig. 2).

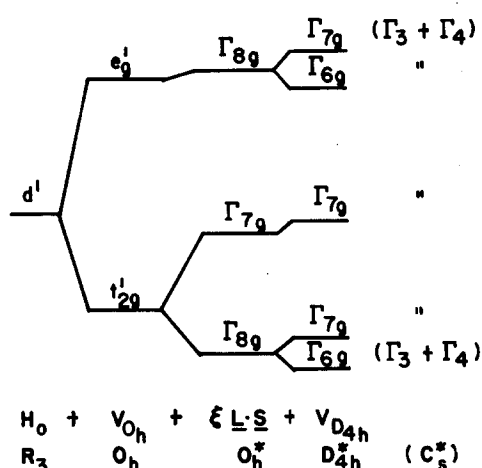One electron wavefunctions and energies applicable

FIG. 1. ReF$_6$ electronic energy level diagram. The model Hamiltonian is given term by term along with the highest symmetry group under whose transformations the Hamiltonian is totally symmetric. The diagram shows the splitting pattern for the highest occupied Re^{+6} orbital under these perturbations. The energy level labels are the irreducible representations for the group given below the Hamiltonian terms. The right hand column gives the rigorous site group representations, although no potential term of this symmetry is directly included in the model.

to the D_{4h} model are obtained by diagonalizing

$$\mathcal{H} = B_4(0\,_4^0 + 50\,_4^4 + 48) + B_2^0 0_2^0 + B_4^0 0_4^0 + \xi(1 \cdot s)$$

$$= V_{0_h} + V_{D_{4h}} + \xi(1 \cdot s) \qquad \text{(III.6)}$$

in the manifold of d-electron states. The $l = 2$ tetragonal basis functions for the octahedral group diagonalize both V_{0_h} and $V_{D_{4h}}$. These functions are listed in Table IV with their transformation properties. The effect of the spin–orbit operator is best calculated after products of spin and orbital functions are reduced. Using the vector coupling coefficients, one obtains 2 Γ_{6g} and 3 Γ_{7g} functions. Table V contains the matrices of the Hamiltonian in this basis. If it is assumed that, under D_{4h} distortion, the $d_z^2(e_g)$ orbital is lower in energy than the $d_{x^2-y^2}(e_g)$ orbital and that the $d_{xz}(t_{2g})$ and $d_{yz}(t_{2g})$ orbitals are lower in energy than the $d_{xy}(t_{2g})$ orbital, the following bounds and conclusion obtain: (1) $B_2^0 > 5\,B_4^0$ and $B_2^0 > -\frac{20}{3}\,B_4^0$; (2) Γ_{6g} is the ground state; and (3) if $[E(\Gamma_{7g}) - E(\Gamma_{6g})]$ is fixed at 30 cm^{-1} (roughly the experimental value), $5 \lesssim B_2^0 \lesssim 100$ cm^{-1}.

TABLE IV. Octahedral group tetragonal basis functions.

Function[a]	Transformation properties D_{4h}	O_h
$\lvert\bar{1}\rangle = \lvert 2 - 1\rangle$	E_g	T_{2g}
$\lvert\bar{0}\rangle = 2^{-1/2}\{\lvert 22\rangle - \lvert 2-2\rangle\}$	B_{2g}	T_{2g}
$\lvert -\bar{1}\rangle = -\lvert 21\rangle$	E_g	T_{2g}
$\lvert\theta\rangle = \lvert 20\rangle$	A_{1g}	E_g
$\lvert\epsilon\rangle = 2^{-1/2}\{\lvert 22\rangle + \lvert 2-2\rangle\}$	B_{1g}	E_g

[a]Notation: $\lvert lm_l\rangle$.

TABLE V. D_{4h} crystal field model electronic Hamiltonian [see Eq. (III.6)].

Γ_{6g} block	$120B_4 - 6B_2^0 + 72B_4^0$	$-\sqrt{\frac{3}{2}}\,\xi$
	$-\sqrt{\frac{3}{2}}\,\xi$	$-\frac{1}{2}\xi - 3B_2^0 - 48B_4^0$

Γ_{7g} block	$120B_4 + 6B_2^0 + 12B_4^0$	$-\xi$	$-\sqrt{\frac{1}{2}}\,\xi$
	$-\xi$	$6B_2^0 + 12B_4^0$	$-\sqrt{\frac{1}{2}}\,\xi$
	$-\sqrt{\frac{1}{2}}\,\xi$	$-\sqrt{\frac{1}{2}}\,\xi$	$\frac{1}{2}\xi - 3B_2^0 - 48B_4^0$

Moffit et al. have shown that in the 0_h molecule, the spectroscopic splitting factor g is zero for Γ_{8g} derived from a pure dt_{2g}^1 configuration. Since $J' = \frac{3}{2}$, $L' = 1$, and $S = \frac{1}{2}$ ($J' = L' + S$) in the Γ_{8g} level, $\mu/\beta (= L + 2S = -L' + 2S) = 0$. This cancellation holds for the D_{4h} model as well, giving $g(\Gamma_{6g}) = 0$. Only mixing of the e_g orbitals into the lower t_{2g} levels via the spin–orbit operator produces significant g values.

Since Γ_{4g}, the irreducible representation of the magnetic moment in 0_h, is contained twice in $[\Gamma_{8g}^* \times \Gamma_{8g}]$, two g values are required to relate the components of μ and J'. In the D_{4h} model the z direction is unique and therefore the expression

$$\mu = g_{\parallel} S_z' \hat{k} + g_\perp (S_x' \hat{i} + S_y' \hat{j}) \qquad \text{(III.7)}$$

may be used within each electronic doublet. The fractionally occupied molecular orbitals in ReF$_6$ are not purely metal orbitals. For ions in crystals, use has frequently been made of orbital reduction factors[16] which reduce the magnitude of the matrix elements of orbital angular momentum operators (i. e., $\mu = \beta(2S + L)$, $\xi L \cdot S$, etc.) between pure metal ion wavefunctions to account for the reduction of metal ion functions in the molecular orbitals. Restricting this parameter to only one value for all types of orbitals, g values are obtained (see Fig. 3) for the lower three doublets of the D_{4h} model as a function of the orbital reduction parameter k.

To aid in the understanding of spectral linewidths, a calculation of the zero-field hyperfine structure of ReF$_6$ was performed. Re has two stable isotopes, ^{185}Re and ^{187}Re, both of which have $I = \frac{5}{2}$ and very similar gyromagnetic ratios ($\gamma \sim 1.12$) and electric quadrupole moments ($Q \sim 2.6$ barn). The hyperfine Hamiltonian for
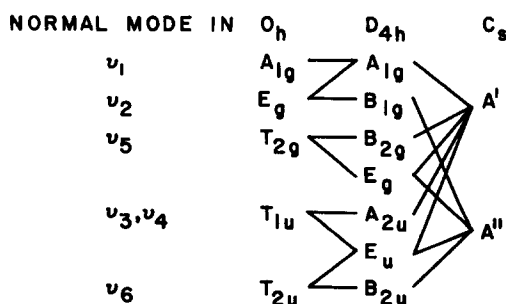

FIG. 2. Correlation diagram appropriate for the normal modes of an octahedral MF$_6$ molecule reduced to D_{4h} or $C_s(\sigma_d)$ symmetry.
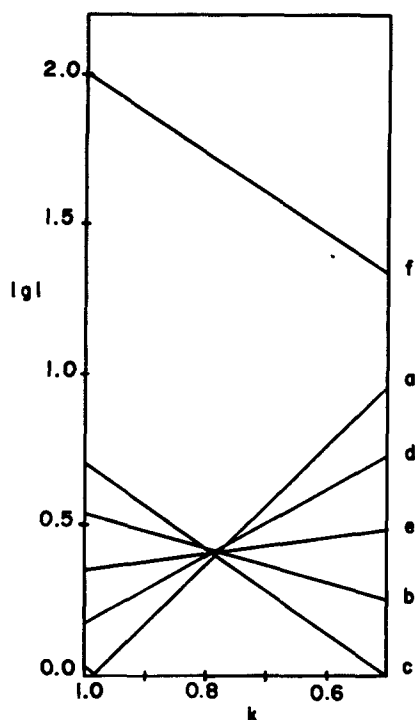
FIG. 3. Spectroscopic splitting factors as functions of the orbital reduction factor in the three lowest levels of ReF_6 — $g_{\parallel}$, $g_{\perp}$, and $\bar{g}$ $(=\tfrac{1}{3}\,[g_{\parallel}+2g_{\perp}])$ are calculated using the wavefunctions which diagonalize the D_{4h} electronic Hamiltonian (III. 6): 120 B_4 $(=10\,D_q)=30\,000$ cm^{-1}; $\xi=3050$ cm^{-1}; and the (octahedral Γ_{8g}) ground state splitting $\delta=30$ cm^{-1}. The results are insensitive to variations of B_2^0 and B_4^0 under this constraint. (a) and (b) are $|g_{\parallel}|$ and $g_{\perp}$ in the Γ_{6g} level; (c) and (d) are $|g_{\parallel}|$ and $g_{\perp}$ in the lower Γ_{7g} level; (e) is $|\bar{g}|$ in both the Γ_{6g} and the lower Γ_{7g} levels; and (f) is $|\bar{g}|$ in the 5000 cm^{-1} 7_{7g} level. $|g_{\parallel}|$ and $g_{\perp}$ differ by only ~ 0.03 in the latter level, making them indistinguishable from $|\bar{g}|$ in this plot.

an electron characterized by l and s and a nucleus characterized by I and Q can be written in standard form (see Ref. 16, for example). Such a calculation is full of difficulties and assumptions dealing with values for $\langle r^{-3}\rangle$, shielding, crystal contributions to the quadrupole terms, etc., but it should serve as a basis for a discussion concerning expected theoretical linewidths and shapes for optical transitions. Diagonalization of the hyperfine Hamiltonian in the three lower electronic levels of the D_{4h} model and the two lower levels of the O_h model yield energy levels given in Table VI. The appropriate parameters are also listed there.

C. Dimers

In mixed crystals with greater than roughly 1% concentration of ReF_6, the probability of statistical dimer or pair formation becomes high. In the hexafluoride structure there are 14 neighbors in the near neighbor sphere (5.21–6.76 Å metal-to-metal distance in UF_6); this corresponds to $\sim 15\%$ probability of dimer formation. The dimer associated absorption may be recognized by its violation of Beer's Law in spectra of different concentration crystals.

In discussing the problem of dimers in molecular crystals the departure point is $\mathfrak{IC}^{site}_{nq}$; we assume that this is the same for all crystals. However, depending on the situation, the $\mathfrak{IC}'$ [see Eqs. (III. 3)–(III. 5)] will change. It is probably most useful to consider these as effective Hamiltonians, particularly for inorganic or open shell systems. In the ReF_6 system, guest–guest interaction terms contain interactions between species with partially filled orbitals. This leads to interactions in the crystal other than van der Waals and resonance interactions typical of organic molecular dimers. Spin coupling or magnetic interactions (electron exchange) now become important. Since discussion of crystal energies and wavefunctions is usually limited to first order in the perturbation scheme, important higher-order effects such as dispersion, kinetic exchange (superexchange), and virtual phonon exchange must be included in an effective Hamiltonian ($\mathfrak{IC}_{eff}=\mathfrak{IC}^0_{eff}$ + $\mathfrak{IC}'_{eff}$) in addition to the electric multipole and potential (direct) exchange which are present in first order.

One-site zero-order wavefunctions can be constructed from antisymmetrized products of the site Hamiltonian eigenfunctions,

$$\varphi^{0\alpha0\alpha}_{nqn'q'}=\mathfrak{a}\,\chi^{0\alpha}_{nq}\chi^{0\alpha}_{n'q'}\prod_{n''q''\neq nq,n'q'}\chi^0_{n''q''}\,, \qquad \text{(III. 8)}$$

in which $\mathfrak{a}$ is the electron antisymmetrizing operator, $\chi^{0\alpha}_{nq}$ is the α "spin" wavefunction of the lowest level of the ReF_6 site, and $\chi^0_{n''q''}$ are the lowest eigenfunctions of the host sites. Dimer functions $\varphi^{0\alpha0\beta}_{nqn'q'}$, $\varphi^{0\alpha0\beta}_{nqn'q'}$, and $\varphi^{0\beta0\beta}_{nqn'q'}$ will be degenerate with (III. 8) in zero order. Excited states of the pair will have zero-order functions of the type

$$\varphi^{f\alpha0\alpha}_{nqn'q'}=\mathfrak{a}\,\chi^{f\alpha}_{nq}\chi^{0\alpha}_{n'q'}\prod_{n''q''\neq nq,n'q'}\chi^0_{n''q''} \qquad \text{(III. 9)}$$

and

$$\varphi^{0\alpha f\alpha}_{nqn'q'}=\mathfrak{a}\,\chi^{0\alpha}_{nq}\chi^{f\alpha}_{n'q'}\prod_{n''q''\neq n'q',nq}\chi^0_{n''q''}\,,$$

in which one of the ReF_6 sites is excited to the fth electronic level. Of course, spin is not conserved in this system, and the α, β notation denotes only partners in a Kramers doublet and not α and β spinors. There is consequently no intersite spin summation rule over these generalized labels so that one may not a priori set a matrix element such as

$$\langle\varphi^{0\alpha0\alpha}_{nqn'q'}\,|\mathfrak{IC}_{eff}|\,\varphi^{0\beta0\beta}_{nqn'q'}\rangle$$

equal to zero even if $\mathfrak{IC}_{eff}$ is a spin-independent two-site operator. Such a selection rule or orthogonality arises only when rotations is real space leave spins unchanged; the levels of two interacting spin one-half systems no longer decompose into a singlet and a triplet.

The situation is quite simple for a spinless system, which has a nondegenerate ground state $\varphi^{00}_{nqn'q'}$ and the usual "exciton" results obtain.[11] The assumption usually made in such a presentation is that both sites are equivalent and therefore matrix elements with nq and $n'q'$ interchanged are identical. This need not be true if the point group of the pair does not contain a

TABLE VI. Calculated hyperfine levels of ReF_6 in the O_h and D_{4h} models. The standard hyperfine Hamiltonian[a] is diagonalized in the four or six lowest energy electronic states of ReF_6 using the parameters 120 B_4 = 30 000 cm^{-1} and ξ = 3200 cm^{-1} to determine the O_h electronic wavefunctions, and the requirement that δ = 30 cm^{-1} for the D_{4h} wavefunctions. The hyperfine parameters are $\langle r^{-3} \rangle$ = 12 a. u. ,[b] $2\beta\beta_N\gamma \langle r_c^{-3} \rangle$ = − 0. 03987 (− 700 kG/unpaired electron),[c] γ = 1.12,[d] and Q = 2. 6 barns.[d]

Energy (cm^{-1})	Symmetry	Energy (cm^{-1})	Symmetry	Energy (cm^{-1})	Symmetry
a. O_h model					
0. 479	Γ_{5g}				
0. 413	Γ_{3g}				
0. 393	Γ_{4g}				
0. 349	Γ_{1g}				
0. 190	Γ_{4g}				
0. 144	Γ_{5g}				
0. 053	Γ_{2g}				
0. 023	Γ_{5g}				
0. 013	Γ_{3g}				
0. 000	Γ_{4g}				
b. D_{4h} model					
0. 306	Γ_{5g}	30. 725	Γ_{1g}	5294. 359	Γ_{3g}
0. 288	Γ_{3g}	30. 725	Γ_{2g}	5294. 355	Γ_{2g}
0. 288	Γ_{4g}	30. 665	Γ_{5g}	5294. 355	Γ_{1g}
0. 270	Γ_{5g}	30. 640	Γ_{4g}	5294. 350	Γ_{5g}
0. 261	Γ_{1g}	30. 474	Γ_{3g}	5294. 254	Γ_{4g}
0. 070	Γ_{2g}	30. 460	Γ_{5g}	5294. 250	Γ_{1g}
0. 050	Γ_{5g}	30. 430	Γ_{1g}	5294. 250	Γ_{2g}
0. 000	Γ_{3g}	30. 430	Γ_{2g}	5294. 238	Γ_{5g}
0. 000	Γ_{4g}	30. 403	Γ_{5g}	5294. 234	Γ_{5g}

[a]See Ref. 16.
[b]G. Perlow, W. Henning, D. Olson, and G. L. Goodman, Phys. Rev. Lett. 23, 680 (1969); J. A. McMillain and T. Halpern, Argonne Natl. Lab. Rep. 7784.
[c]A. J. Freeman, J. V. Mallow, and P. S. Bagus, J. Appl. Phys. 41, 1321 (1970).
[d]J. E. Mack, Rev. Mod. Phys. 22, 64 (1950).

symmetry operation which interchanges the pair sites. However, for the spinless case one can view this as approximately true for a weak coupling ("infinite dilution" wavefunction) limit.

For dimers of ReF_6, the "magnetic" interactions (electron exchange) complicate the above simple picture. Owing to various anisotropic exchange mechanisms, large spin–orbit coupling, and in general, rigorous inequivalence of the two sites comprising the dimer, the four degenerate zero-order states $\varphi_{nqn'q'}^{0\alpha 0\alpha}$ will yield four nondegenerate first-order dimer states. In the block corresponding to functions degenerate in zero order with $\varphi_{nqn'q'}^{0\alpha f\alpha}$, there will be $4m$ nondegenerate first-order dimer states, where m is the degeneracy of the fth excited site state. If excitation exchange is vibronically forbidden, the $4m \times 4m$ block decomposes into two $2m \times 2m$ blocks. Generalized matrix elements in this problem have the form

$$M_{nqn'q'}^{0\alpha f\alpha 0\beta f\alpha} \equiv \langle \varphi_{nqn'q'}^{0\alpha f\alpha} | \mathcal{H}'_{eff} | \varphi_{nqn'q'}^{0\beta f\alpha} \rangle$$

$$= \langle \alpha \chi_{nq}^{0\alpha} \chi_{n'q'}^{f\alpha} | \mathcal{H}'_{eff} | \alpha \chi_{nq}^{0\beta} \chi_{n'q'}^{f\alpha} \rangle . \quad (\text{III. 10})$$

These matrix elements will also be useful in the decomposition of the pure crystal exciton band.

The problem of two ReF_6 molecules imbedded in a host crystal lattice is in general quite complex. The Hamiltonian is invariant under operations of time in-

version and the subgroup symmetry of the $Pnma$ space group not destroyed by the substitution of two ReF_6 molecules for two host molecules in the crystal. The possible dimer symmetry groups are C_s, C_i, and C_1. Much simplification of the dimer energy matrix occurs if the wavefunctions are made to transform according to these symmetries where they are applicable. C_s pairs are created when both ReF_6 molecules substitute for host molecules on the same crystal mirror plane or when ReF_6 molecules are separated by a translation in the b direction only. The number of ways to form C_i pairs is too great to list, but an example in one unit cell would be ReF_6 at sites I and III or II and IV.

While the site symmetry is rigorously reduced in C_i and C_1 pairs, the zero-order ReF_6 site functions may be chosen to be the infinite dilution functions which are characterized by the irreducible representations of the group C_s. For pairs with C_s symmetry, the antisymmetrized product wavefunctions which form the zero-order basis may be combined to transform as Γ_1 or Γ_2 of C_s. For pairs with C_i symmetry, the inversion operator can be considered to be an interchange operator (i. e., $C_i \Gamma_3^I = \Gamma_3^{II}$, $C_i \Gamma_4^I = \Gamma_4^{II}$ with Γ_3, Γ_4 belonging to C_s), and combinations of the antisymmetrized product functions may be selected to transform as Γ_1 or Γ_2 of C_i. Matrix element selection rules can be used to set half the elements of $\mathcal{H}$ equal to zero. The great-

TABLE VII. Matrices of the effective pair Hamiltonian within the zeroth order degenerate blocks of the dimer (see text, Sec. III. B, for fuller discussion of terms, approximations, and assumptions).

A. Both sites unexcited

Wavefunctions:

$$|a\rangle = 2^{-1/2}(\phi_{12}^{0\alpha 0\alpha} + \phi_{12}^{0\beta 0\beta})$$

$$|b\rangle = 2^{-1/2}(\phi_{12}^{0\alpha 0\beta} - \phi_{12}^{0\beta 0\alpha})$$

$$|c\rangle = 2^{-1/2}(\phi_{12}^{0\alpha 0\alpha} - \phi_{12}^{0\beta 0\beta})$$

$$|d\rangle = 2^{-1/2}(\phi_{12}^{0\alpha 0\beta} + \phi_{12}^{0\beta 0\alpha})$$

Hamiltonian:

	$|a\rangle$	$|b\rangle$	$|c\rangle$	$|d\rangle$
	A	E	$-iG$	$-iJ$
	E	B	$-iH$	$-iK$
	iG	iH	C	F
	iJ	iK	F	D

C_1 pair: general case—10 parameters

C_i pair: E, H, $K = 0-7$ parameters

C_s pair (inequivalent sites): E, F, H, $J = 0-6$ parameters

C_s pair (equivalent sites): E, H, $K = 0-7$ parameters

B. One site excited

Wavefunctions:

$$|a\rangle = 2^{-1}(\phi_{12}^{0\alpha f\alpha} + \phi_{12}^{0\beta f\beta} + \phi_{12}^{f\alpha 0\alpha} + \phi_{12}^{f\beta 0\beta})$$

$$|b\rangle = 2^{-1}(\phi_{12}^{0\alpha f\beta} - \phi_{12}^{0\beta f\alpha} + \phi_{12}^{f\alpha 0\beta} - \phi_{12}^{f\beta 0\alpha})$$

$$|c\rangle = 2^{-1}(\phi_{12}^{0\alpha f\alpha} + \phi_{12}^{0\beta f\beta} - \phi_{12}^{f\alpha 0\alpha} - \phi_{12}^{f\beta 0\beta})$$

$$|d\rangle = 2^{-1}(\phi_{12}^{0\alpha f\beta} - \phi_{12}^{0\beta f\alpha} - \phi_{12}^{f\alpha 0\beta} + \phi_{12}^{f\beta 0\alpha})$$

$$|e\rangle = 2^{-1}(\phi_{12}^{0\alpha f\alpha} - \phi_{12}^{0\beta f\beta} + \phi_{12}^{f\alpha 0\alpha} - \phi_{12}^{f\beta 0\beta})$$

$$|f\rangle = 2^{-1}(\phi_{12}^{0\alpha f\beta} + \phi_{12}^{0\beta f\alpha} + \phi_{12}^{f\alpha 0\beta} + \phi_{12}^{f\beta 0\alpha})$$

$$|g\rangle = 2^{-1}(\phi_{12}^{0\alpha f\alpha} - \phi_{12}^{0\beta f\beta} - \phi_{12}^{f\alpha 0\alpha} + \phi_{12}^{f\beta 0\beta})$$

$$|h\rangle = 2^{-1}(\phi_{12}^{0\alpha f\beta} + \phi_{12}^{0\beta f\alpha} - \phi_{12}^{f\alpha 0\beta} - \phi_{12}^{f\beta 0\alpha})$$

Hamiltonian:

	$|a\rangle$	$|b\rangle$	$|c\rangle$	$|d\rangle$	$|e\rangle$	$|f\rangle$	$|g\rangle$	$|h\rangle$
	A	I	J	L	ia	ie	ij	in
	I	B	K	M	ib	if	ik	ip
	J	K	C	N	ic	ig	il	iq
	L	M	N	D	id	ih	im	ir
	$-ia$	$-ib$	$-ic$	$-id$	E	P	Q	S
	$-ie$	$-if$	$-ig$	$-ih$	P	F	R	T
	$-ij$	$-ik$	$-il$	$-im$	Q	R	G	U
	$-in$	$-ip$	$-iq$	$-ir$	S	T	U	H

C_1 pair: general case—36 parameters

C_i pair, C_s pair (equivalent sites: I, J, M, N, Q, R, S, T, b, c, f, g, j, m, n, $r = 0-20$ parameters

C_s pair (inequivalent sites): I, K, L, N, P, R, S, U, b, d, e, g, k, m, n, $q = 0-20$ parameters

C. One excited site but with zero vibrational overlap to the ground state.

Hamiltonian: same as in B.

C_1 pair: reduction of matrix element values—none are zero *a priori*

TABLE VII (*Continued*)

C. One excited site but with zero vibrational overlap to the ground state

C_i pair, C_s pair (equivalent sites): $A = C$, $B = D$, $E = G$, $F = H$, $K = L$, $U = P$, $a = l$, $e = q$, $d = k$, $h = p -$ 10 parameters

C_s pair (inequivalent sites): $A = C$, $B = D$, $E = G$, $F = H$, $a = l$, $c = j$, $f = r$, $h = p - 12$ parameters.

est simplification arises for C_i and for the special case of C_s with neither partner on the mirror, in which case it is rigorously true that $M_{nqn'q'}^{0\alpha f\alpha 0\beta f\alpha} = M_{nqn'q'}^{f\alpha 0\alpha f\alpha 0\beta}$; nonetheless, presence of both electron and excitation exchange does not allow for a completely reduced form.

The Hamiltonian is also invariant under the operation of time reversal Θ.[16,17] If basis functions are combined so as to display the spatial symmetry just described and to transform symmetrically or antisymmetrically under time inversion, then $\langle \psi | \mathcal{K} | \psi' \rangle = \pm \langle \psi | \mathcal{K} | \psi' \rangle^*$ (the plus sign holding for both ψ and ψ' transforming similarly under time reversal and the minus holding otherwise). Since time reversal symmetric and antisymmetric functions belong to the same corepresentation of the time reversal group, the only requirement on Hamiltonian matrix elements imposed by time reversal symmetry is that they be either real or pure imaginary. The total number of parameters required to describe interactions within a zero-order degenerate block for different pair symmetries is thus easily determined. These are listed in Table VII along with the forms of the matrices.

D. Neat crystal

Molecular exciton theory is well developed and has been presented in many forms over the years,[11] and energies, wavefunctions, and matrix elements can be written down in the Frenkel approximation. We need to discuss, however, the two added complications that occur in inorganic molecular crystals like ReF_6: paramagnetic crystals and magnetically ordered crystals. Further, in this instance, applicability of the restricted Frenkel limit[18] is questionable. This useful limit in effect assumes interactions between certain translationally equivalent molecules are either zero or equal and thus $k \neq 0$ exciton branches which diagonalize $\mathcal{K}_{eff}$ are constructed from the one-site exciton functions by the same prescription as the $k = 0$ exciton branches. Since, in the hexafluoride structure, nearest neighbors occupy translationally equivalent sites in the c direction, the restricted Frenkel limit is expected not to apply. It also follows that dispersion for exciton branches should be larger than their separation.

It is possible to develop an energy level structure for magnetically ordered ReF_6 crystals based on the pair parameters if it is assumed that pair interactions are responsible for the ordering and excitation exchange phenomena. If the ordered crystal has all

sites equivalent (not necessarily always true, but *assumed* to be true here), the ground state can be described by the site functions $\chi_{nq}^{0\alpha}$. The problem of equivalent sites is somewhat difficult in the ordered crystals, as the interchange group may be antiunitary. The crystal functions are then given as,

$$\varphi^0 = a \prod_{nq} \chi_{nq}^{0\alpha} \ ,$$

$$\varphi_{nq}^{f\alpha} = a \ \chi_{nq}^{f\alpha} \prod_{nq \neq n'q'} \chi_{n'q'}^{0\alpha} \ . \tag{III.11}$$

Since choice of interchange operators phases one site coordinate system (spin and space) relative to the others, these functions can correspond to ferromagnetic, antiferromagnetic, or canted (scew) magnetic ordering even though they all have the same Kramers component label. $\varphi_{nq}^{f\alpha}$ and $\varphi_{nq}^{f\beta}$ are degenerate in zero order. The diagonal energies of the localized states are

$$\mathcal{E}^{f\alpha} = \langle \varphi_{nq}^{f\alpha} | \mathcal{K}_{eff} | \varphi_{nq}^{f\alpha} \rangle - \mathcal{E}^0$$

$$= \epsilon^f + \sum_{n'q' \neq nq} (M_{nqn'q'}^{f\alpha 0\alpha f\alpha 0\alpha} - M_{nqn'q'}^{0\alpha 0\alpha 0\alpha 0\alpha})$$

$$= \overline{\epsilon}^f + \Delta^{f\alpha} \ , \tag{III.12}$$

and

$$\mathcal{E}^{f\beta} = \epsilon^f + \sum_{n'q' \neq nq} (M_{nqn'q'}^{f\beta 0\alpha f\beta 0\alpha} - M_{nqn'q'}^{0\alpha 0\alpha 0\alpha 0\alpha})$$

$$= \overline{\epsilon}^f + \Delta^{f\beta} \ . \tag{III.13}$$

In these two equations, ϵ^f is the difference in site energies between the ground and excited states, $\overline{\epsilon}^f$ is this difference in the gas phase, $\mathcal{E}^0$ is the ground state energy, and $\Delta^{f\alpha}$ is the so-called gas-to-crystal shift.[11] $\mathcal{E}^{f\alpha}$ will not in general equal $\mathcal{E}^{f\beta}$. The above admonition concerning antiunitary interchange groups is important here if one wishes to compare M's obtained from pair spectra or calculations with those derived for neat crystals (i.e., the α, β indices must be carefully treated for a proper comparison). Exciton functions can be constructed as in the spinless cases. If $f=0$ and α and β indices are changed, magnon functions will arise. The effective Hamiltonian matrix elements then take the usual form

$$\langle \varphi_q^{f\alpha}(\mathbf{k}) | \mathcal{K}_{eff} | \varphi_{q'}^{f'\beta}(\mathbf{k}) \rangle = \mathcal{L}_{qq'}^{f\alpha f\beta}(\mathbf{k}) + \mathcal{E}^0 \delta_{qq'} \delta_{ff'} \delta_{\alpha\beta}$$

$$= L_{qq'}^{f\alpha f'\beta}(\mathbf{k}) + (\mathcal{E}^0 + \overline{\epsilon}^f + \Delta^{\alpha f}) \delta_{qq'} \delta_{ff'} \delta_{\alpha\beta} \ , \tag{III.14}$$

in which the possibility is foreseen that mixing between exciton bands will be important. This is particularly true if $\varphi_q^{f\alpha}(\mathbf{k})$ and $\varphi^{f\beta}(\mathbf{k})$ are considered different bands. The $L_{qq'}^{f\alpha f'\beta}(\mathbf{k})$ may be expressed in terms of the M's

$$L_{qq'}^{f\alpha f'\beta}(\mathbf{k}) = \sum_n e^{i\mathbf{k}\cdot(\mathbf{R}_{0q'}-\mathbf{R}_{nq})} M_{nq_0 0q'}^{f\alpha 0\alpha 0\alpha f\beta} \ . \tag{III.15}$$

If the interactions are short range, the summation over sites may be truncated. If only the 14 molecule near neighbor sphere around a site (I for example) is considered, it is necessary to use one $I-I'$, two I-II, one I-IV, and two I-III interaction parameters *for each isolated* $\chi^{f\alpha}$ *level*. For $\mathbf{k}=0$,
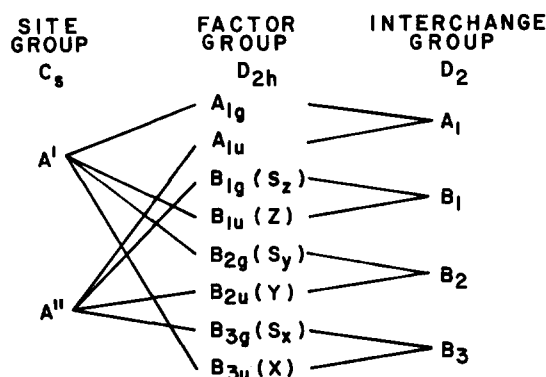

FIG. 4. Correlation diagram among groups pertinent to the ReF$_6$ ($Pnma$-D_{2h}^{16}) crystal. Components of R and S, position and rotation vectors (electric and magnetic dipoles), are also listed.

$$L_{I-I'}^{f\alpha f\beta}(0) = 2M_{I-I'}^{f\alpha 0\alpha 0\alpha f\beta} \ ,$$

$$L_{I-II}^{f\alpha f\beta}(0) = 2\,M_{I-II}^{f\alpha 0\alpha 0\alpha f\beta} + 2\,M_{I-II'}^{f\alpha 0\alpha 0\alpha f\beta} \ ,$$

$$L_{I-III}^{f\alpha f\beta}(0) = 2\,M_{I-III}^{f\alpha 0\alpha 0\alpha f\beta} + 2\,M_{I-III'}^{f\alpha 0\alpha 0\alpha f\beta} \ , \tag{III.16}$$

$$L_{I-IV}^{f\alpha f\beta}(0) = 4\,M_{I-IV}^{f\alpha 0\alpha 0\alpha f\beta} \ .$$

The usual exciton theory then proceeds via group theory to obtain algebraic $\mathbf{k}=0$ exciton energy levels, but this further reduction is not generally possible for both electron exchange (energy localizing terms) and excitation exchange (energy delocalizing) interactions. The situation is identical to that described for the dimers. Separation into $\mathbf{k}$-state blocks still occurs, but exact diagonalization of these blocks by the factor group operations is not always possible even for $\mathbf{k}=0$.

Well above the transition temperature for magnetic ordering ReF$_6$ crystals are paramagnetic. In the absence of an external magnetic field, the average value of any component of the magnetic moment is zero. Since the spins are randomly oriented and fluctuating, the crystal cannot be described by a wavefunction. An incoherent superposition of states, the density matrix, must be employed. It is possible, however, to speak of crystal excitations (Frenkel excitons) and to label them by the operators which create them.[19] The $\mathbf{k}=0$ excitons transform as irreducible representations of the factor group (isomorphic to) D_{2h}. This factor group is the direct product of the site group C_s and the proper interchange group (isomorphic to) D_2 (three mutually perpendicular sets of twofold screw axes and the identity). Since the electronic excitations at a site may be either A' or A'' in C_s (caused by the variability of spin orientation in both initial and final states), g and u $\mathbf{k}=0$ excitons will be degenerate. Figure 4 contains the appropriate correlation diagrams between site, factor, and interchange groups. Since there are four molecules in the unit cell, four exciton bands (transforming as A, B_1, B_2, and B_3 in D_2) are expected. Both dipole operators transform as $B_1 + B_2 + B_3$ in D_2, therefore only three pure exciton branches are expected to be observed in the optical spectra.

Below the magnetic ordering temperature the magnetic moments will have well defined equilibrium directions. Deviations from these directions in the absence of electronic excitation are described as magnons. Loudon[19] has shown that in magnetically ordered crystals, exciton and magnon descriptions are formally identical (see above as well). Unlike Loudon, however, we will use the magnetic space group to describe excitations.

The transformation properties of crystal wavefunctions in the Shubnikov (magnetic or "black and white") group of the crystal are a convenient means of labeling. The wavefunctions will transform as irreducible corepresentations of the space group.[20] If we restrict our interest to $k=0$ excitations, a considerable amount of complexity can be avoided.

Assuming ReF_6 magnetically orders with no loss of atomic positional symmetry and that spins align in keeping with that symmetry, the magnetic space group for the ordered crystal must be one that can be derived from D_{2h}^{16} $(Pnma)$. There are seven of these in addition to $Pnma$ itself.[21] The unit cell sizes of all of these magnetic space groups are the same as for the paramagnetic crystal. The reason for this is that any one of the primitive translation operators of the space group is equivalent to the square of one of the twofold screw operations. Whether the twofold screw becomes unitary or antiunitary in the magnetic group, its square must be unitary. Three of the groups require antiferromagnetic order, one requires ferromagnetic order, two allow canted magnetic order requiring zero residual moment, and two allow canted order with residual moments varying from zero to the ferromagnetic value. These magnetic groups, their various subgroups, and correlation diagrams are presented in Fig. 5. Below, we discuss some considerations which should make this figure more understandable and useful.

In analogy to space groups, one may define factor groups for the seven nontrivial Shubnikov groups of interest here. The concept of factor groups as direct products of site and interchange groups is also a useful concept where applicable. Since these factor groups are all antiunitary, the $k=0$ exciton wavefunctions are classified according to the irreducible corepresentations for which they form bases. Since for these seven groups single valued corepresentations are all such that no degeneracy is required by the presence of antiunitary operators[20b,c], $k=0$ exciton wavefunctions may be classified as irreducible representations of unitary subgroups of index 2 of the factor group. The same situation holds for site and interchange groups. Correlation diagrams between site, interchange, and factor groups become correlation diagrams between the largest unitary groups contained in them.

In using the correlation diagrams, certain facts are useful: (1) crystal wavefunctions are single valued even when site wavefunctions are double valued because the ground state is in any event totally symmetric and the direct product of two double valued representations
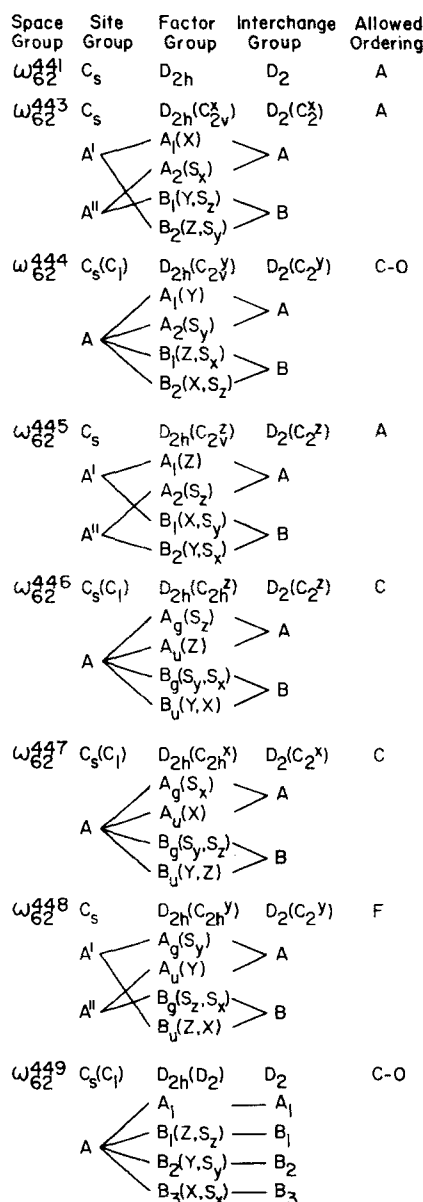

Space Group	Site Group	Factor Group	Interchange Group	Allowed Ordering
ω_{62}^{441}	C_s	D_{2h}	D_2	A
ω_{62}^{443}	C_s	$D_{2h}(C_{2v}^x)$	$D_2(C_2^x)$	A

FIG. 5. Correlation diagrams among corepresentations of Shubnikov groups appropriate to possible magnetic ordering in the ReF_6 crystal. The Shubnikov space group notation is that of Ref. 21. For the finite black and white groups, the notation lists the unitary subgroup of index two in parenthesis with superscript identifying the appropriate unitary axis. Components of position and rotation vectors, R and S, are listed with the irreducible corepresentations according to which they transform. The allowed magnetic orderings in the space groups are indicated by F, A, C-0, or C for ferromagnetic, antiferromagnetic, canted with residual magnetic moment equal to zero or canted with arbitrary residual moment variable between zero and the full ferromagnetic value. Shubnikov group ω_{62}^{441} consists of only unitary elements, and consequently the correlation diagram is that of Fig. 4. ω_{62}^{442} contains the time reversal operator as an element and therefore does not describe magnetically ordered crystals.

(or corepresentations) is single valued; (2) symmetry species of transition operators label excitations; (3) to create four linearly independent exciton functions from antiunitary interchange groups, one-site excitation functions are combined using irreducible repre-

sentations of the unitary group obtained by treating antiunitary operators as unitary operators. This latter point implies that for the hexafluorides under consideration, one-site ($k=0$ exciton) functions are combined with four sets of coefficients from the irreducible representations of D_2 (the point group isomorphic to all the "unitarized" interchange groups). In the antiunitary group, some of these functions may transform as the same irreducible corepresentation. For the D_2 (C_2) antiunitary interchange group, there will be two functions transforming as the A and two functions transforming as the B irreducible corepresentations.

Functions transforming as the same row of an irreducible corepresentation may mix under the influence of a totally symmetric Hamiltonian. Therefore the $k=0$ exciton functions are not uniquely (unambiguously) determined. The symmetries are useful, however, for obtaining selection rules and polarizations. Selection rules may be worked out based on the unitary subgroups of index 2 of the factor group. Figure 5 shows the various relations, along with transformation properties of the components of electric and magnetic dipole operators.

This analysis leads to the conclusion that the electronic origin of the ReF_6 $t_{2g} - t_{2g}$ transition at 5000 cm^{-1}, in the Frenkel limit, should contain eight exciton branches at least six of which are $E1$ or $M1$ allowed (see Figs. 4 and 5). The transition should remain mostly of magnetic dipole nature; some "forced electric dipole" character could come about through crystal mixing. In the event of exciton–phonon and/or exciton–magnon coupling, the $\Delta k = 0$ optical selection rule may still be satisfied by $k \neq 0$ excitons in combination with $k \neq 0$ phonons or magnons. Phonon or magnon side bands are commonly encountered in, respectively, molecular crystals[22] and magnetically ordered (ionic) inorganic crystals.[23]

E. Two-molecule or two-particle transitions

Finally, we wish to discuss a phenomenon very distinctly portrayed in these systems, two-molecule or two-particle transitions. Such transitions involve two sites; one site is electronically excited, and a (presumably) neighboring site is vibrationally excited. This transition is easily distinguished from one-site vibronic transitions in that its energy is that of the electronic origin of the guest (ReF_6) plus a *ground state* vibration on the *host* (either the same chemical species ReF_6 or MoF_6, WF_6, or UF_6). These transitions are present throughout this series.

Two mechanisms have been proposed by which such states can gain intensity. The first is based on host–guest interaction via mixing of a guest electronic state with an electronic exciton band of the host.[24] The major area of application of this mechanism has been to isotopic mixed organic systems. The mixing of states or delocalization of guest transitions is a function of $\Delta_e (= \epsilon_h^f - \epsilon_g^f)$, the electronic binding energy of the trap or the binding energy of the exciton localized on the impurity center; $\Delta_{ev} = (\nu_h' - \nu_g')$, the host–guest ex-

cited state vibrational energy difference; Δ_{ex} = host exciton bandwidth; and $\Delta_\nu = (\nu_g' - \nu_h'')$, which is the "vibrational defect" defined as the difference between the guest excited state vibration (ν_g') and the host ground state vibration (ν_h''). For substantial (>5%) two-particle intensity in the spectrum, it is necessary that $\Delta_{ex} > |\Delta_\nu|$ and $\Delta_{ex} > \Delta_e$. When $|\Delta_\nu| \approx \frac{1}{2}\Delta_{ex}$, most (~98%) of the intensity resides in one-particle or vibronic single-site transitions.

The second mechanism, proposed for two-ion simultaneous transitions in ionic crystals,[25] is based on the mixing of one-site transitions with two-site transitions through the intermolecular potential. It does not depend on the presence of exciton bands or crystal states in general. The state with which the two molecule state mixes in order to get optical intensity would, in this instance, be the one-site vibronic state of the guest. While this may not be the state of greatest oscillator strength, it is the one for which the energy separation is smallest. This mechanism is not unlike what has been called "intermolecular Fermi resonance" in vibrational spectra of organic molecular crystals.[26]

In trying to apply these mechanisms to two-molecule transitions or states observed in mixed and pure ReF_6 crystals, it would appear that the first mechanism is inapplicable since Δ_e is at least 20 000 cm^{-1} and as much as 55 000 cm^{-1}. However, it is also possible to think of ground state host vibrations as the enabling exciton bands. The exact experimental situation and intensities can be used to decide between these and perhaps other possibilities, as will be discussed below.

IV. EXPERIMENTAL

Transition metal hexafluorides are highly volatile ($P \sim 200$ mm at 300 K), air-sensitive compounds and must thus be handled in high vacuum apparatus. While both fluorine and hexafluorides are inert with respect to Pyrex and quartz, HF will autocatalytically attack the silica/hexafluoride and is difficult to remove in the early states of F_2 handling, synthesis, and sample preparation. Thus, all manipulations prior to the final sample distillation into the optical cell are performed in monel vacuum systems that have been "pickled" or passivated at high temperature with H_2 and F_2.[27] Both gases were purified by slow distillation through liquid nitrogen traps, and in the case of fluorine large excesses of the liquid were trapped and the first and last fractions were always discarded. Operating pressures in the vacuum manifolds are typically in the 10^{-6} torr range.

The ReF_6 used in these studies was either obtained from Dr. J. Malm of Argonne National Laboratory or was synthesized from 99.99% pure Re powder (D. F. Goldsmith Co., Evanston, IL) and F_2 (Matheson Gas Co.). The powder used for the synthesis was loaded into a previously passivated and evacuated monel reaction vessel in an inert atmosphere dry box. After evacuation, the powder was degassed by slowly raising the temperature to 300 °C under vacuum maintained for at least 12 h at this temperature (pressure $\approx 1 \times 10^{-6}$

torr). The main system was repassivated with the Re metal isolated in the reaction can, and distilled fluorine was admitted to the system. The pressure in the reaction vessel was kept below 5 atm at the 300 °C reaction temperature, and an excess of Re metal was maintained to prevent formation of ReF_7. Purification of ReF_6 from more and less volatile contaminants was accomplished by trap-to-trap sublimation while pumping. The collection trap was cooled by a diethyl ether slush.

UF_6 was obtained from Varlacoid (Elizabeth, NJ), and MoF_6 and WF_6 were obtained from ROC/RIC (Sun Valley, CA). These material were purified by trap-to-trap sublimation in a separate manifold used only for manipulation of host (closed shell) compounds. This precaution was necessary to avoid possible cross contamination between various paramagnetic hexafluorides begin studied in this laboratory. After purification these materials were stored in monel vessels which could easily be removed and attached to other manifolds. Host cans were maneuvered so as to avoid exposure of their valves to measurable pressures of other hexafluorides.

Quartz sample cells were attached to the manifolds through graded seals to Pyrex, Pyrex-to-copper Housekeeper seals, and finally copper-to-monel vacuum brazed joints. Cells were heated to 450 °C and pumped ($P \sim 5 \times 10^{-7}$ torr) for at least 24 h before use. Components for the various mixed crystals (ReF_6 in MoF_6, WF_6, or UF_6) were measured by admitting a known pressure of gas into a calibrated volume. Pressures were measured with a monel bourdon type gauge or obtained from vapor pressure vs temperature data.[28] Each sample was separately metered and sublimed into the sample cell to avoid fractionation. 200–300 torr of helium gas, dried by slow passage through a liquid nitrogen cooled trap, was admitted into the cold sample cell. The cells would then be sealed off the system below the graded seal.

All crystals were grown from the vapor. A cooled copper wire contacted the cell where crystal was desired. Depending on the size and shape of the sample cell, growth was completed in a period of 3 weeks to 3 months. Single crystals roughly $2 \times 2 \times 2$ cm in rectangular quartz cells could be grown by this method. UF_6 crystals were grown at room temperature, and ReF_6, MoF_6, and WF_6 crystals were grown in a -20 °C cold room below the cubic–orthorhombic phase transition. Samples were cooled to 77 K by lowering them at speeds ranging from 7.5–15 cm/day into liquid nitrogen. Some cracking of the crystals usually occurred during this latter stage, but often only 2 or 3 cracks would develop in the $2 \times 2 \times 2$ cm crystals.

Spectra were taken with the samples immersed in either boiling nitrogen, boiling helium, or superfluid helium (~ 1.5 K). Samples, especially at 1.5 K bath temperature, were probably somewhat warmer than this even though there was 1–5 mm of He in the cell at 2 K. Thin, pure crystal samples (0.1–1.0 mm) were probably below 2 K when the bath temperature was 1.5 K. Low resolution spectra (5–6 cm^{-1} slits) were obtained on a Cary 14 R (IR-2 option). The 2.0 μ band

of HBr and the 1.8 μ band of HCl[29] were used to calibrate the instrument. For higher resolution, a 0.5 m scanning double monochromator (McPherson Model 285) with two 600 grooves/mm gratings blazed at 1.85 μ was used. Since this is a single-beam setup, water must be excluded from the monochromator and light path by N_2 flushing. The higher resolution ir system is designed around a Texas Instruments 2×4 mm liquid nitrogen cooled InAs detector. The detector and matching zero-biasing preamp (Perry Amplifier Co., Brookline, MA) are contained in an aluminum Faraday cage mounted at the exit slit of the monochromator. The light source is a GE 1958 or 1959 tungsten iodine lamp operated at constant current by a stabilized dc power supply and filtered with IR-85 and G-533 or B-460 glass filters from Hoya Glass Co. The system band pass before the monochromator was 1–2.5 μ.

In order for the photo voltaic detector to operate well it must see an ac signal of a frequency somewhere between 400 Hz and 50 MHz. This has been accomplished by two techniques: intensity (amplitude) modulation of the source with a frequency-locked light chopper or frequency modulation by a quartz wedge optical scanner (American Time Products) mounted at the exit slit of the double monochromator. In both cases the modulation frequency was roughly 400 Hz. The chopper gives the full absorption spectrum, while the modulator gives a signal that approximates the first derivative of the absorption. The position of the sample with respect to either modulation scheme is irrelevant. The detector signal is then amplified by the preamp and a lock-in amplifier (PAR HR-8 with a type C plugin). The output of the HR-8 is recorded on a two pen strip chart recorder as either the absorption spectrum or its first derivative. Since the noise limiting feature of the system is detector noise, the method of modulation is important only in that the sensitivity of the system changes with modulation method. With full beam amplitude modulation the detector always sees a large ac signal (that is, the lock-in amplifier must be kept on a low gain scale), whereas the frequency modulation scheme gives no signal for no absorption in the light path. Typical weak signal readings for the FM scheme are on the 20 μV scale but on the 0.5 mV scale for the AM scheme. In the former situation, the limiting signal-to-noise ratio (sensitivity) is due to detector noise, and in the latter case it is due to amplifier overload. On the other hand, for weak broad features the AM technique is better.

The other pen of the two pen strip chart recorder marks wavelength as determined by a microswitch attached to the monochromator's drive screw. This mechanism was calibrated over the 1.7–2.0 μ range with $H^{35}Cl$, $H^{37}Cl$, H_2O, $H^{79}Br$, and $H^{81}Br$[29]. The correction curve was adequately fitted by a least squares method to an expression which was the sum of a straight line and a sine wave with a period equal to the revolution period of the monochromator's drive screw. The standard deviation for this fit is $\sigma = 0.09$ Å, and the over-all accuracy of reported data or mean error (3σ) is roughly 0.07 cm^{-1} at 2.0 μ. The smallest attainable slits in this region while taking low temperature crystal

FIG. 6. Low resolution absorption spectra of various ReF$_6$ containing crystals near 2K. The crystal are (a) neat ReF$_6$, (b) 3% ReF$_6$ in UF$_6$, (c) 2% ReF$_6$ in WF$_6$, and (d) 2% ReF$_6$ in MoF$_6$. Typical slitwidths are 5–6 cm^{-1}. Transitions to some excited state vibrational levels common to all crystals are identified over the neat crystal spectrum.

spectra are 50 μm or 0.2 cm^{-1}.

Optical spectra were obtained for pure crystals of ReF$_6$, for crystals containing 0.3%, 0.8%, 3%, and 10% mole fraction of ReF$_6$ in UF$_6$, and 0.3%, 1.0%, and 2% mole fraction of ReF$_6$ in MoF$_6$ and WF$_6$. These samples varied in thickness from 0.05 mm to 2 cm.
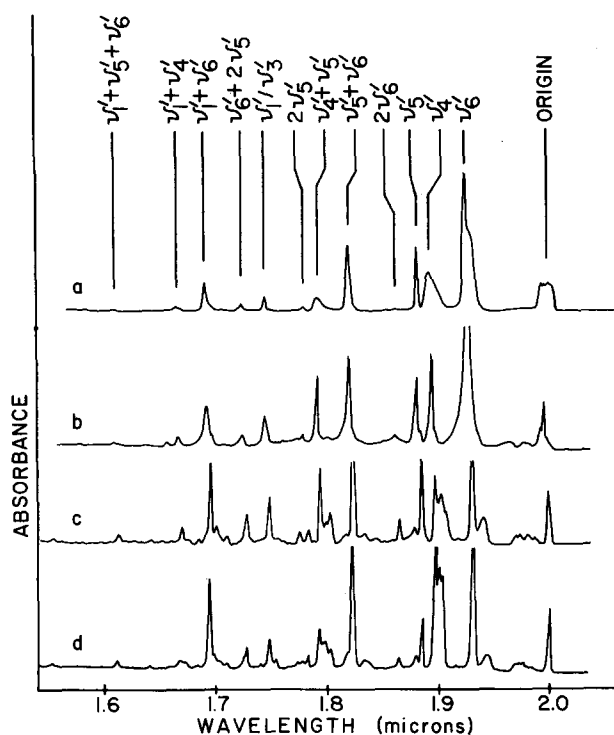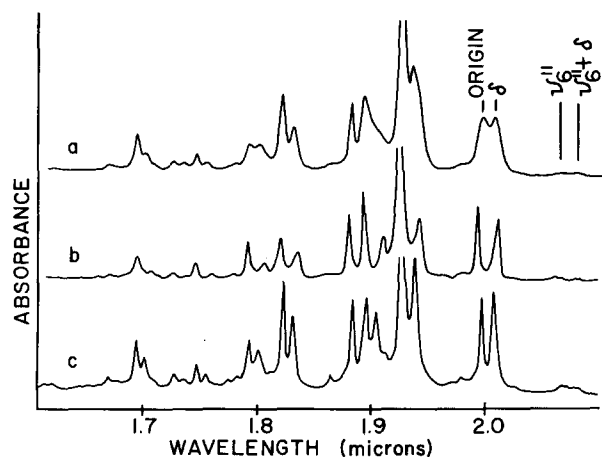

FIG. 7. Low resolution absorption spectra of various ReF$_6$ containing crystals near 77 K. The crystals are (a) neat ReF$_6$, (b) 3% ReF$_6$ in UF$_6$, and (c) 2% ReF$_6$ in WF$_6$. Typical slit widths are 5–6 cm^{-1}. The origin splitting and ν_6'' vibrational hot bands are indicated.
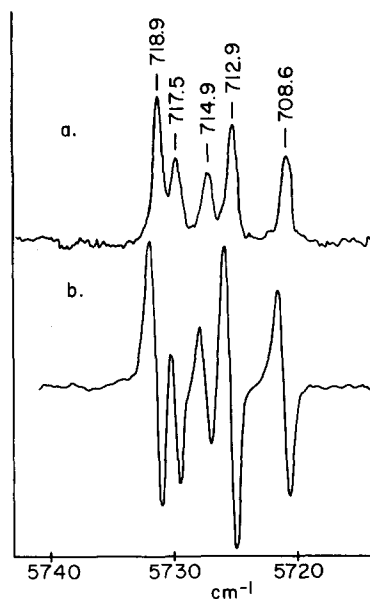
FIG. 8. High resolution spectra of the ν_1'/ν_3' region of ReF$_6$ in UF$_6$ at 2 K. (a) and (b) were obtained by the amplitude and frequency modulation techniques, respectively. Slitwidths are between 0.3 and 0.4 cm^{-1}. Section IV of the text discusses these two experimental techniques.

Magnetic susceptibility measurements were performed at Bell Laboratories (with Dr. F. J. Di Salvo) using a technique described elsewhere.[30]

V. RESULTS

Representative low resolution spectra of the various crystal systems are displayed in Figs. 6 and 7. Portions of the high resolution spectra are presented in Figs. 8–10 and 12–14. Data obtained from pure and various concentration mixed crystals are presented in Tables VIII and IX. Spectra obtained from crystals of the same chemical composition but different concentrations differed only in linewidth and concentration dependent pair peaks. The tabulated results are generally averages over many measurements on different crystals. The exception to this pattern is a sharp feature occurring on the red edge of the pure crystal origin at helium temperature (see Fig. 14). Having ob-
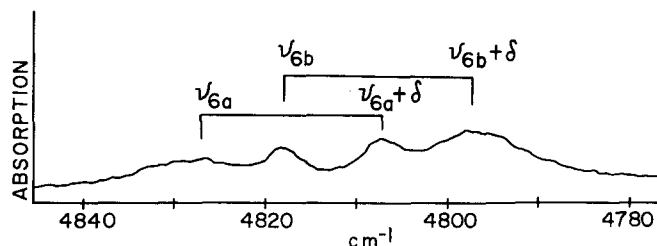
FIG. 9. Hot band spectra of ReF$_6$ and MoF$_6$ involving ν_6''. The site splittings of the ν_6'' (t_{2u}) vibration and the Γ_{8g} electronic ground state of the octahedral molecule are portrayed. While energetics make the interpretation clear, line shapes are not consistent. Lifetime and/or vibronic coupling effects in the lower manifolds may be responsible for these differences. The site splitting of ν_6'' is given by $|\nu_{6a}'' - \nu_{6b}''| \sim 10$ cm^{-1}.
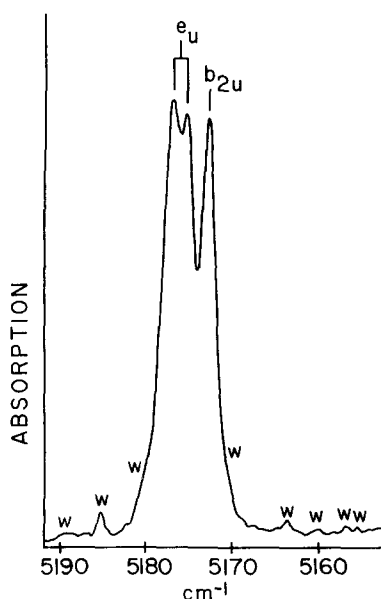
FIG. 10. Site splitting of the octahedral ν_6' vibration of ReF_6 in MoF_6. The components are labeled by irreducible representations of the approximate D_{4h} site group. Slitwidth was 0.35 cm^{-1}.

tained a crystal with favorable orientation, we could alter the relative intensity of this peak drastically by rotating the crystal relative to the light beam.

Even though the optical path was flushed with dry nitrogen gas, weak water peaks appeared in spectra in the region from 5150–5500 cm^{-1}. These sharp features are easily identified by comparison to atmosphere tracings and are labeled by "w" in the figures of this paper.

The magnetic susceptibility measured between 10–300 K is summarized by the expression

$$\chi_M = 69 \times 10^{-4}/T + 0.69 \times 10^{-4} \text{ emu-deg/mole.}$$

Below 10 K the behavior is complex and is discussed in Sec. VI. F.

VI. DISCUSSION

A. General vibronic features

The main features of the $\Gamma_{7g} \rightarrow \Gamma_{6g}$ (D_{4h}) transition of ReF_6 in the various crystals are molecular in nature. The low resolution spectra are interpreted in terms of the six vibrations of an octahedral molecule (Tables VIII and IX). Intensity distribution in totally symmetric $\nu_1'(\sim 715 \text{ cm}^{-1})$ progressions indicates a minimal shift of equilibrium position. The origin and its progressions are magnetic dipole allowed with some crystal field induced $E1$ character due to destruction of the molecular inversion center at the crystal site. The $\nu_4'(t_{1u})$ at 270 cm^{-1} and $\nu_6'(t_{2u})$ at 180 cm^{-1} modes serve as false origins largely via Herzberg–Teller coupling. Progressions in $\nu_5'(t_{2g})$ at (300 cm^{-1}) are in part due to Jahn–Teller (pseudo-Jahn–Teller in the D_{4h} and C_s models) activity of the ground state. Combinations and overtones up to a total of three or four quanta are observed. Anharmonicities, as measured from the low

resolution combination and overtone band centers, are small—typically less than 1 cm^{-1}/added quantum.

Under higher resolution, peaks involving ν_4', ν_5', ν_6' are observed to split. The splitting is consistent with a D_{4h} model with a small C_s symmetry field superimposed. For example, vibronic peaks of threefold degenerate octahedral fundamentals are interpreted as though their vibrations split into singly and doubly degenerate modes in D_{4h} symmetry (see Fig. 2); the doubly degenerate mode is split to a lesser extent by the C_s distortion. Figures 10 and 13 show this vibrational splitting in several hosts.

The assignment of all resolved features in the combination and overtone bands is complicated by possible anharmonicity and Fermi resonance effects. The later effect is important considering the reduced site symmetry and the close spacing of the split components of the degenerate octahedral modes. The assignments in Table VIII are based on the best energy and intensity matchings, assuming mixing and splitting of harmonic D_{4h} combination and overtone levels by the crystal potential are small.

While vibronic spectra in the bending region (ν_4, ν_5, ν_6) are straightforward and assignments are certain, considerable ambiguity exists in the stretching (ν_1, ν_2, ν_3) region at ~ 700 cm^{-1}. The peak that appears to correspond to a totally symmetric vibration (ν_1) at ~ 715 cm^{-1} in WF_6 and MoF_6 mixed and ReF_6 pure crystals is observed as three distinct features in ReF_6/UF_6 mixed crystals in low resolution. Only one of these ReF_6/UF_6 peaks matches the energy of the vibration apparently involved in combination bands. This same feature is the one that builds on these three peaks to give observed "$2\nu_1'$" band structure in low resolution (see Table VIII). At highest resolution, the "ν_1" peaks are seen to be somewhat asymmetric in the other hosts, but no splitting has been discerned. Owing to two-particle transitions, UF_6 is the best host for the study of one particle (vibron) spectra in this region. Assignment of the two intense "additional" peaks in ReF_6/UF_6 as components of ν_3' is supported by the occurrence of ν_3 in the ground state at ~ 715 cm^{-1} in the vapor phase. The e_u and a_{2u} components in the D_{4h} model would be identified with the 718.1 and 708.0 cm^{-1} features, respectively, based on the roughly 2:1 intensity ratio and the expected smaller force constant for the a_{2u} axial mode. Linewidths in MoF_6 and WF_6 crystals are significantly narrower than this splitting; therefore, for these mixed crystals ν_3' and ν_1' are assigned as degenerate. This indicates, as do the ground state splittings discussed below, that the D_{4h} distortion is largest for ReF_6/UF_6 mixed crystals.

Figure 8 displays this region in high resolution. The assignment of the 718.1 cm^{-1} low resolution peak as the e_u split component of $\nu_3'(t_{1u})$ would be supported by the observed 1.4 cm^{-1} splitting. However, the occurrence of two peaks at 712.9 and 714.9 cm^{-1} then makes the ν_1' assignment uncertain. The $2\nu_4' + \nu_6'$ and $4\nu_6'$ bands are expected in this region and may gain intensity through Fermi resonance with ν_1'/ν_3'. Indeed, the relative intensities of the features at 718.9, 712.9, and 708.5

TABLE VIII. Summary of the spectra of mixed and neat crystal of ReF_6 at ~ 1.5 K. Frequencies are listed as cm^{-1} from the origins. Absolute origin transition frequencies are listed in parentheses. The neat crystal frequencies are given as cm^{-1} from the 0–0 total exciton band center at 5009.5 cm^{-1} as discussed in the text, Sec. VI. E. Frequency uncertainties are ± 0.1 cm^{-1} for sharp lines. Relative peak heights are scaled to a constant number of absorbers in the path. Pair peaks are measured in 2% ReF_6/MoF_6 and WF_6 samples and 0.8% ReF_6/UF_6 samples.

Frequency (cm⁻¹)	Intensity[a]	FWHH(cm⁻¹)	Assignment
(a) ReF_6 in MoF_6			
−6.2	M		
−5.4	W		pair
−3.3	S		
−1.9	M		
0(4995.4)	S	0.7	origin
1.3	M		
2.2	S		
2.7	S		
3.7	M		pair
4.7	W		
5.8	M		
7.6	W		
40.0[b]	W		
60.3[b]	W		phonon
76.2[b]	W		
135.6	W		
141.0	M	21	ν_6' (host)
146.5	M		
152.6	W		
165.2	W		
168.5	W		pair
170.4	M		
177.4	S		$\nu_6'(b_{2u})$
180.0	S	6.4	$\nu_6'(e_{ua})$
181.5	S		$\nu_6'(e_{ub})$
191.9	M		pair
247.2	M		
251.4	M		
254.0	S		
259.5	S		ν_4'' (host)
262.0	S		
263.7	M		
265.1	S		
270.9	S		$\nu_4'(a_{2u})^c$
272.4	M		$\nu_4'(e_u)^c$
274.1	S		
302.4	S	5.1	$\nu_5'(e_g)$
303.8	S		$\nu_5'(b_{2g})$
315.1	M		
318.0	M	9	ν_5'' (host)
320.7	M		
356.1	W		$2\nu_6'(b_{2u})$
359.6	M		$\nu_6'(b_{2u}) + \nu_6'(e_{ua})$
361.1	M		$\nu_6'(b_{2u}) + \nu_6'(e_{ub})$, $2\nu_6'(e_{ua})$
362.8	W		$\nu_6'(e_{ua}) + \nu_6'(e_{ub})$
364.5	M		$2\nu_6'(e_{ub})$
432.6	W		
441.6	M	26	$\nu_5' + \nu_6''$ (host)
452.2	M		$\nu_4' + \nu_6'$
459.7	W		
478.3	S		$\nu_5'(e_g) + \nu_6'(b_{2u})$

Frequency (cm⁻¹)	Intensity[a]	FWHH (cm⁻¹)	Assignment
(a) ReF_6 in MoF_6			
481.3	S		$\nu_5'(b_{2g}) + \nu_6'(b_{2u})$
482.3	S	4.5	$\nu_5'(e_g) + \nu_6'(e_{ua})$
484.1	S		$\nu_5'(e_g) + \nu_6'(e_{ub})$, $\nu_5'(b_{2g}) + \nu_5'(e_{ua})$
486.6	S	1.6	$\nu_5'(b_{2g}) + \nu_6'(e_{ub})$
495.3	M		
498.1	M		ν_5'' (host) $+ \nu_6'$
501.7	W		
539.8	M		
541.4	M		
543.7	M		
545.1	M		$2\nu_4'$, $3\nu_8'$
547.1	M		
548.6	M		
557.4	S		
565.4	M		ν_4'' (host) $+ \nu_5'$
574.3	S		$\nu_4'(a_{2u}) + \nu_5'^c$
577.1	S		$\nu_4'(e_u) + \nu_5'^c$
590.5	W		$\nu_4' + \nu_5''$ (host)
604.9	M		$2\nu_5'(e_g)$
606.5	M	5.2	$\nu_5'(e_g) + \nu_5'(b_{2g})$
608.2	M		$2\nu_5'(b_{2g})$
621.0	M	14	$\nu_6' + \nu_5''$ (host)
636.1	M	10	$\nu_4' + 2\nu_6'$
644.8	M	11	ν_2'' (host)
650.6	W		
661.0	M	5.2	$\nu_5' + 2\nu_4'$
664.1	W		
693.9	M		ν_3'' (host)
696.5	M		
718.2	S	6.8	ν_1', ν_3', $2\nu_4' + \nu_6'$, $4\nu_6'^d$
741.6	M	1.0	ν_1'' (host)
779.2	M		
782.3	M		
784.0	M		
787.3	M		$2\nu_5' + \nu_6'$
790.4	W		
791.5	M		
795.3	VW		
801.0	W		$\nu_5' + \nu_5''$ (host) $+ \nu_6'$
839.9	M		
842.9	M	10	$2\nu_4' + \nu_5'$, $\nu_5' + 3\nu_6'$
846.8	M		
862.0	M	≥17	$\nu_1' + \nu_6''$ (host)
880.7	M		$\nu_4' + 2\nu_5'$
892.7	S	11	$\nu_1'/\nu_3' + \nu_6 (b_{2u})$
896.6	S		$\nu_1'/\nu_3' + \nu_6'(e_u)$
906.8	W		
911.7	W		$3\nu_5'$
913.4	W		
930.8	VW		
933.3	W		$\nu_4' + \nu_5' + 2\nu_6'$
935.0	W		

TABLE VIII (*Continued*)

(a) ReF_6 in MoF_6

Frequency (cm⁻¹)	Intensity[a]	FWHH (cm⁻¹)	Assignment
974.9	M	}	$\nu_1'/\nu_3' + \nu_4''$ (host)
991.4	M	} 36	$\nu_1'/\nu_3' + \nu_4'$
997.5	W	}	
1018.6	W	10	$\nu_1'/\nu_3' + \nu_5'$
1043.9	W	} 3.0	ν_1'' (host) $+ \nu_5'(e_g)$
1045.4	W	}	ν_1'' (host) $+ \nu_5'(b_{2g})$
1056.1	W		$\nu_4' + 2\nu_5' + \nu_6'$
1089.0	W	≥ 20	$\nu_6' + 3\nu_5',\ \nu_1'/\nu_3' + 2\nu_6'$
1198.3	M	9.1	$\nu_1'/\nu_3' + \nu_5' + \nu_6'$
1257.7	VW		$\nu_1'/\nu_3' + 2\nu_4',\ \nu_1'/\nu_3' + 3\nu_6'$
1430.8[b]	W		$2\nu_1'/\nu_3'$
1496.3[b]	VW		$\nu_1'/\nu_3' + 2\nu_6' + \nu_6'$
1620.9[b]	W	18	$2\nu_1'/\nu_3' + \nu_6'$

(b) ReF_6 in WF_6

Frequency (cm⁻¹)	Intensity[a]	FWHH (cm⁻¹)	Assignment
−6.2	W		}
−5.0	M		}
−4.5	M		} pair
−3.3	W		}
−2.0	M		}
0. (5000.0)	S	0.9	origin
2.1	S		}
3.4	W		}
4.2	M		} pair
5.9	W		}
7.0	W		}
34.9[b]	W		}
50.1[b]	W		} phonon
68.5[b]	W		}
77.3[b]	W		}
154.6	M	21	ν_6'' (host)
167.3	W		
170.4	W		}
172.7	M		} pair
173.8	M		}
177.3	S	} 6.8	$\nu_6'(b_{2u})$
180.6	S	}	$\nu_6'(e_u)$
186.4	W		pair
242.6	M		
251.1	S		}
252.3	S		}
255.0	M		} ν_4'' (host)
256.0	W		}
264.8	S		}
269.0	S	1.4	$\nu_4'(e_u)$
271.7	S	1.3	$\nu_4'(a_{2u})$
273.1	M		}
274.7	W		} pair
276.0	M		}
302.4	S	} 5.7	$\nu_5'(e_g)$
304.0	S	}	$\nu_5'(b_{2g})$
320.8	M	}	}
322.2	M	} 7	} ν_5'' (host)
324.5	M	}	}
355.3	M		$2\nu_6'(b_{2u})$

TABLE VIII (*Continued*)

(b) ReF_6 in WF_6

Frequency (cm⁻¹)	Intensity[a]	FWHH (cm⁻¹)	Assignment
359.1	W	}	} $\nu_6'(b_{2u}) + \nu_6'(e_u)$
360.3	M	} 3.2	}
362.2	W	}	} $2\nu_6'(e_u)$
363.6	M	}	}
452.2	W		} $\nu_4' + \nu_6'$
453.7	W		}
478.0	M		$\nu_5'(e_g) + \nu_6'(b_{2g})$
481.7	S		$\nu_5'(b_{2g}) + \nu_6'(b_{2g})$
484.1	S		$\nu_5'(e_g) + \nu_6'(e_u)$
486.5	S		$\nu_5'(b_{2g}) + \nu_6'(e_u)$
499.2	W		}
502.3	W		} ν_5'' (host) $+ \nu_6'$
505.3	W		}
534.3	VW		
538.7	M		; $2\nu_4'(e_u)$
539.6	W		
541.3	M		; $\nu_4'(e_u) + \nu_4'(a_{2u})$
542.6	M		
543.9	M		$3\nu_6'$; $2\nu_4'(a_{2u})$
545.8	M		
546.9	M		
548.5	VW		
549.4	VW		
552.1	W		ν_4'' (host) $+ \nu_5'$
554.5	W		
556.0	W		
557.6	W		
567.4	W		
571.7	S		$\nu_4'(e_u) + \nu_5'(e_g)$
573.2	S	} 5.6	$\nu_5'(e_u) + \nu_5'(b_{2g}),\ \nu_4'(a_{2u}) + \nu_5'(e_g)$
575.9	M		$\nu_4'(a_{2u}) + \nu_5'(b_{2g})$
591.6[b]	VW		$\nu_4' + \nu_5''$ (host)
605.7	W	}	$2\nu_5'(e_g)$
607.1	W	} 6.3	$\nu_5'(e_g) + \nu_5'(b_{2g})$
608.8	W	}	$2\nu_5'(b_{2g})$
629.6	W	}	}
631.8	W	} 6.0	} $\nu_4' + 2\nu_6'$
633.0	M	}	}
635.3	VW		
660.9[b]	VW		$\nu_5' + 2\nu_6'$
716.7	S	5.6	$\nu_1',\ \nu_3',\ 2\nu_4' + \nu_6',\ 4\nu_6'$[d]
771.7	M	1.1	ν_1'' (host)
778.9	W		}
783.5	M		} $2\nu_5' + \nu_6'$
787.7	M		}
791.4	M		}
838.8	W		}
841.8	W		} $2\nu_4' + \nu_5',\ 3\nu_6' + \nu_5'$
845.8	W		}
849.0	W		}
877.9	M		} $\nu_4' + 2\nu_6',\ \nu_1'/\nu_3' + \nu_6''$ (host)
882.3	W		}
893.0	M	} 7.6	$\nu_1'/\nu_3' + \nu_6'(b_{2u})$
896.4	S	}	$\nu_1'/\nu_3' + \nu_6'(e_u)$
903.9	VW		$2\nu_4' + 2\nu_6'$

TABLE VIII (*Continued*)

Frequency (cm⁻¹)	Intensity[a]	FWHH (cm⁻¹)	Assignment
(b) ReF$_6$ in WF$_6$			
907.3	VW		$3\nu_5'$
930.7	W		
933.4	W		$\nu_4' + \nu_5' + 2\nu_6'$
934.4	W		
964.2[b]	VW		$\nu_1'/\nu_3' + \nu_4''$ (host)
985.7	W		$\nu_1'/\nu_3' + \nu_4'$ (e_u)
987.9	M	5.8	$\nu_1'/\nu_3' + \nu_4'$ (a_{2u})
989.6	VW		
991.4	VW		
1020.6[b]	VW		$\nu_1'/\nu_3' + \nu_5'$
1048.3[b]	VW		
1089.9[b]	VW		$\nu_1'/\nu_3' + 2\nu_6', \ \nu_6' + 3\nu_5'$
1193.0	W		
1198.2	W		$\nu_1'/\nu_3' + \nu_5' + \nu_6'$
1203.0	W		
1256.5[b]	VW		$\nu_1'/\nu_3' + 2\nu_4', \ \nu_1'/\nu_3' + 3\nu_6'$
1292.3[b]	VW		$\nu_1'/\nu_3' + \nu_4' + \nu_5'$
1321.8[b]	VVW		$\nu_1'/\nu_3' + 2\nu_5'$
1347.4[b]	VVW		$\nu_1'/\nu_3' + \nu_4' + 2\nu_6'$
1432.8[b]	W		$2\nu_1'/\nu_3'$
1487.9[b]	VW		$\nu_1'/\nu_3' + 2\nu_5' + \nu_6'$
1610.6[b]	W	14	$2\nu_1'/\nu_3' + \nu_6'$
1698.3[b]	VW		$2\nu_1'/\nu_3' + \nu_4'$
1733.5[b]	VW		$2\nu_1'/\nu_3' + \nu_5'$
1910.8[b]	VW		$2\nu_1'/\nu_3' + \nu_5' + \nu_6'$
(c) ReF$_6$ in UF$_6$			
−16.0	M		
−14.1	W		
−12.5	M		
−12.0	W		
−10.2	W		pair
−8.1	M		
−7.5	M		
−3.6	M		
−2.0	M		
0. (5012.5)	S	1.1	origin
5.1	W		
6.0	M		
6.4	W		
8.2	M		pair
9.7	M		
10.7	M		
41.2[b]	W		phonon
79.1[b]	W		
152.3	W		ν_6'' (host)
160.6	M		
173.3	S		
175.6	S		$\nu_6'(e_u)$[a]
178.8	S		$\nu_6'(b_{2u})$[a]
181.6	S		ν_4'' (host)
185.1	M		
194.5	M		
202.9	M		
206.2	M		ν_5'' (host)
214.2	W		
219.5	W		

TABLE VIII (*Continued*)

Frequency (cm⁻¹)	Intensity[a]	FWHH (cm⁻¹)	Assignment
(c) ReF$_6$ in UF$_6$			
254.1	M		
257.2	M		pair
261.3	M		
265.1	S	5.5	$\nu_4'(e_u)$
268.2	S		$\nu_4'(a_{2u})$
269.7	S		
274.4	M		pair
276.9	M		
279.9	M		
290.9	W		pair
292.7	VW		
299.2	W		
302.2	S	3.8	$\nu_5'(e_g)$
304.3	S		$\nu_5'(b_{2g})$
306.8	VW		
308.2	W		pair
310.7	M		
313.2	W		
351.7	W		$2\nu_6'(e_u)$[c]
357.6	W		$2\nu_6'(b_{2u})$[c]
474.6	M		$\nu_5' + \nu_4''$ (host)
477.8	S		$\nu_5'(e_g) + \nu_6'(e_u)$[c]
480.6	S		$\nu_5'(b_{2g}) + \nu_6'(e_u), \ \nu_5'(e_g) + \nu_6'(b_{2u})$[c]
483.2	S		$\nu_5'(b_{2g}) + \nu_6'(b_{2u})$[c]
491.8	W		
494.7	W		$\nu_5' + \nu_4''$ (host)
499.9	W		
502.5	VW		$\nu_6' + \nu_5''$ (host)
506.1	VW		
517.1	VW	≳12	ν_2'' (host)
535.3	W		$2\nu_4', \ 3\nu_6'$
567.1	S		$\nu_4'(e_u) + \nu_5'(e_g)$
568.3	S	5.6	$\nu_4'(e_u) + \nu_5'(b_{2g})$
570.7	M		$\nu_4'(a_{2u}) + \nu_5'(e_g)$
572.7	M		$\nu_4'(a_{2u}) + \nu_5'(b_{2g})$
604.9	M		$2\nu_5'(e_g)$
607.3	W		$\nu_5'(e_g) + \nu_5'(b_{2g})$
609.1	M		$2\nu_5'(b_{2g})$
625.2	VW		$2\nu_6' + \nu_4'$
664.5	M	1.4	ν_1'' (host)
708.6	M	1.3	$\nu_3'(a_{2u})$[d]
712.9	S	1.3	ν_1'[d]
714.9	M		$\nu_6' + 2\nu_4', \ 4\nu_6'$[d]
717.5	M		
718.9	S	1.3	$\nu_3'(e_u)$[d]
774.9	VW		
778.0	W		
781.9	M		$2\nu_5' + \nu_6'$
787.7	M		
795.5	W		$3\nu_4'$
805.8	VW		
870.5	M		$\nu_4'(e_u) + 2\nu_5'(e_g),$ $\nu_4'(e_u) + \nu_5'(e_g) + \nu_5'(b_{2g})$
872.6	W		$\nu_4'(a_{2u}) + 2\nu_5'(e_g)$
875.0	M		$\nu_4'(e_u) + 2\nu_5'(b_{2g}), \ \nu_4'(a_{2u}) + \nu_5'(e_g)$ $\nu_5'(b_{2g}), \ \nu_4'(a_{2u}) + 2\nu_5'(b_{2g})$

TABLE VIII (*Continued*)

Frequency (cm⁻¹)	Intensity[a]	FWHH (cm⁻¹)	Assignment
(c) ReF₆ in UF₆			
884.0	M		
891.6	M		
894.3	M		$\nu_6' + \nu_1'$, $\nu_6' + \nu_3'$,
897.2	M		$2\nu_4' + 2\nu_6'$, $3\nu_5'$,
901.1	M		Two-particle transition
907.4	W		
912.7	W		
915.2	W		
929.2	VW		$\nu_4' + \nu_5' + 2\nu_6'$
973.7	M		$\nu_4'(e_u) + \nu_3'(a_{2u})$
977.4	M		$\nu_4'(e_u) + \nu_1'$, $\nu_4'(a_{2u}) + \nu_3'(a_{2u})$
980.6	M		$\nu_4'(e_u) + 714.9$, $\nu_4'(a_{2u}) + \nu_1'$
982.9	M		$\nu_4'(e_u) + 717.5$, $\nu_4'(e_u) + \nu_4'(e_u)$, $\nu_4'(a_{2u}) + 714.9$
986.7	M		$\nu_4'(a_{2u}) + 717.5$, $\nu_4'(a_{2u}) + \nu_3'(e_u)$
1010.4	W		$\nu_5'(e_g) + \nu_3'(a_{2u})$
1012.6	W		$\nu_5'(b_{2g}) + \nu_3'(a_{2u})$
1014.7	W		$\nu_5'(e_g) + \nu_1'$
1016.6	M		$\nu_5'(e_g) + 714.9$, $\nu_5'(b_{2g}) + \nu_1'$
1019.3	W		$\nu_5'(e_g) + 717.5$, $\nu_5'(b_{2g}) + 714.9$
1020.9	VW		$\nu_5'(e_g) + \nu_3'(e_u)$, $\nu_5'(b_{2g}) + 717.5$
1023.1	W		$\nu_5'(b_{2g}) + \nu_3'(e_u)$
1080.0[b]	VVW		$\nu_1' + 2\nu_6'$
1095.3[b]	VVW		
1173.9[b]	VVW		$\nu_4' + 3\nu_5'$
1192.7[b]	VW		$\nu_1' + \nu_5' + \nu_6'$
1316.5[b]	VVW		$\nu_1' + 2\nu_5'$
1420.3[b]	W		$\nu_1' + \nu_3'(a_{2u})$
1426.1[b]	W		$2\nu_1'$
1430.7[b]	W		$\nu_1' + \nu_3'(e_u)$
1598.1[b]	VW	21	$2\nu_1' + \nu_6'$
1605.6[b]	VW		
(d) ReF₆ (neat)[b]			
−4.4	S	38	Observed origin[e]
170.7	S	21	ν_6''
184.4	VS		ν_6'
271.7	S	31	ν_4', ν_4'', ν_5''
302.3	S	7	ν_5'
331.5	VW		
338.6	VW		
359.1	W		$2\nu_6'$
381.9	VW		
440.1	VW		
482.2	VS		$\nu_5' + \nu_6'$
569.0	M	23	$\nu_4' + \nu_5'$
607.9	W	11	$2\nu_5'$
625.9	W	21	$\nu_4' + 2\nu_6'$
659.8	VW		$\nu_5' + 2\nu_6'$
691.8	VW	21	
716.5	M	8	ν_1'/ν_3'
784.7	M		$2\nu_5' + \nu_6'$
792.8	M		
840.8	W		$\nu_5' + 3\nu_6'$, $2\nu_4' + \nu_5'$
893.5	S	13	$\nu_1'/\nu_3' + \nu_6'$
914.5	VVW		
934.5	VW		$\nu_4' + \nu_5' + 2\nu_6'$

TABLE VIII (*Continued*)

Frequency (cm⁻¹)	Intensity[a]	FWHH (cm⁻¹)	Assignment
(d) ReF₆ (neat)[b]			
983.5	W	23	$\nu_1'/\nu_3' + \nu_4'$
1019.1	VW		$\nu_1'/\nu_3' + \nu_5'$
1055.3	VW		
1089.7	VW		
1198.3	W		$\nu_1'/\nu_3' + \nu_5' + \nu_6'$
1430.0	W		$2\nu_1'/\nu_3'$
1499.5	VW		$\nu_1'/\nu_3' + 2\nu_5' + \nu_6'$
1609.9	VW		$2\nu_1'/\nu_3' + \nu_6'$
1694.2	VW		$2\nu_1'/\nu_3' + \nu_4'$
1732.7	VVW		$2\nu_1'/\nu_3' + \nu_5'$
1911.4	VVW		$2\nu_1'/\nu_3' + \nu_5' + \nu_6'$

[a] W = weak, M = medium, S = strong, V = very.
[b] Measured in low resolution; frequency uncertainties are ± 0.5 cm⁻¹.
[c] The assignment is an approximation due to the overlap of single-particle and two particle bands (see Table X).
[d] See text (Sec. VI. A).
[e] Calculated from the exciton band center at 5009.5 cm⁻¹ as discussed in text, Sec. VI. E.

cm⁻¹ vs those of the 717.5 and 714.9 cm⁻¹ features are consistent with identification of the latter as induced absorptions in a weak resonance. In the $\nu_1'/\nu_3' + \nu_5'$ (and $\nu_1'/\nu_3' + \nu_4'$) band, it appears that the e_g (e_u) and b_{2g} (a_{2u}) components of ν_5' (ν_4') add to all five peaks (see Table X). Consideration of the energies of the $2\nu_1$ region in low resolution supports the conclusion that the 712.9 cm⁻¹ peak is ν_1', in the limit of weak resonance.

There are no moderately intense peaks which can be identified as components of $\nu_2'(e_g)$. All other features in the energy region of ν_2' or ν_2' plus bending modes can be accounted for as combinations and overtones of ν_1', ν_3', ν_4', ν_5', and ν_6' (one- and two-particle transitions).

B. Ground state properties—hot band spectra

The splitting δ of the ReF₆ $\Gamma_{8g}(O_h)$ ground state has been measured from electronic hot bands in the various crystals at 77 K. If complications arising from exciton band structure, exciton density of states, and phonon coupling are neglected, the value of δ in the paramagnetic pure crystal may be taken to be the difference in energy of the two observed pure electronic optical band centers; then, δ = 26.8 cm⁻¹ for the pure crystal. In mixed crystals, this electronic splitting is found to be δ(Re/Mo) = 24.2 cm⁻¹; δ(Re/W) = 24.6 cm⁻¹; and δ(Re/U) = 45.9 cm⁻¹.

Electronic hot bands are broader than the true origins. The low energy $\Gamma_{7g}(D_{4h})$ lies within the phonon "continua" at 77 K, and the increased linewidth may be due to lifetime broadening through phonon coupling. An indication of the extent of phonon coupling in these systems is the amount of intensity occurring in phonon side bands of the 2 K spectra. For the MoF₆, WF₆, and UF₆ mixed crystal origins, these intensity ratios, normalized to an origin intensity of 1 are, respectively, 0.71, 0.95, and 1.18. If one assumes that the 77 K

TABLE IX. Summary of ReF_6 neat and mixed crystal spectra at 77 K. Frequencies are given in cm⁻¹ from the respective origins. Absolute transition frequencies for mixed crystal origins are listed in parentheses. The neat crystal transition energies are listed as cm⁻¹ from the 0—0 total exciton band center located at 5003.7 cm⁻¹ as discussed in Sec. VI. E. of the text.

Δν (cm⁻¹)	FWHH (cm⁻¹)	I	Δν (cm⁻¹)	FWHH (cm⁻¹)	I	Δν (cm⁻¹)	FWHH (cm⁻¹)	I	Δν (cm⁻¹)	FWHH (cm⁻¹)	I	Assignment
ReF_6/MoF_6			ReF_6/WF_6			ReF_6/UF_6			ReF_6			
									−199.9		W	$-\delta - \nu_6''$
−198.5		W	−203.3		W	−216.4		W				$-\delta - \nu_{6b}''$
−189.1		W	−192.4		W	−204.8		W				$-\delta - \nu_{6a}''$
									−169.3		W	$-\nu_6''$
−176.8		W	−177.6		W	−178.1		W				$-\nu_{6b}''$
−167.0		W	−168.9		W	−166.4		W				$-\nu_{6a}''$
			−70.3		W							$\nu_6' - \nu_5''$
−24.2	7	S	−24.6	14	S	−45.9	14	M	−30.8		M	$-\delta$
0. (4996.4)	6	S	0. (5000.6)	8	S	0. (5014.7)	8	M	−4.0ᵃ [5003.7]		M	Origin
14.3		W										$\nu_6' - \nu_{6a}''$
						33.4	31	W				
			53.9		W				46.5 }	54	W	Phonons
			69.0		W				68.7 }		W	Phonons
						77.1	39	W				$\nu_5' - \nu_6'' - \delta$, phonons
120.5		W										$\nu_5' - \nu_6''$
						133.2		S				$\nu_8' - \delta, \nu_5' - \nu_6''$
155.8	10	VS	153.4		VS				150.6		S	$\nu_6' - \delta$
179.3	10	VS	180.1		VS	177.1	13	VS	179.2	20	VS	ν_6'
			224.8		W							
233.7		W										
255.9 }		S	244.8	13	M	218.4		M				$\nu_4' - \delta$
	30		269.7	12	S							ν_4'
272.8 }		S				265.7	9	S	271.1	26	M	$\nu_4', \nu_5' - \delta$
302.4	7	M	303.2	8	S	303.0	9	M	302.0	13	M	ν_5'
317.9		W										$\nu_5' + \nu_6' - \nu_{6a}''$
336.3		VW										$2\nu_6' - \delta$
358.6		W	357.8	11	W	354.1	57	W	350.7	43		$2\nu_6'$
						434.9	22	M				$\nu_5' + \nu_6' - \delta, 2\nu_5' - \nu_{6a}''$
458.3	11	M	456.1	13	M				452.1	21	M	$\nu_5' + \nu_6' - \delta$
482.5	11	S	483.0		S	480.7	16	M	481.8	17	M	$\nu_5' + \nu_6'$
						523.1	17	W	542.3		W	$\nu_4' + \nu_5' - \delta$
542.0		M										$2\nu_4', 3\nu_6', \nu_1' - \nu_{6b}''$
			546.3	19	M							$\nu_1' - \nu_{6a}'', \nu_4' + \nu_5' - \delta, 3\nu'_6$
554.3		M										$\nu_4' + \nu_5' - \delta, \nu_1' - \nu_{6a}''$
572.8		M										$\nu_4' + \nu_5'$
			574.5	14	M	567.6	11	M	570.8		W	$\nu_4' + \nu_5', 2\nu_5' - \delta$
605.6		W				606.5		W	604.9		W	$2\nu_5'$
			605.7		W							$2\nu_5', \nu_4' + 2\nu_6' - \delta$
			629.4		W							$\nu_4' + 2\nu_6'$
695.2	12	W	692.3		W	667.8		W	687.2		W	$\nu_1' - \delta$
716.7	10	M	717.3	11	M	716.7	13	M	717.6	15	W	ν_1' [b]
760.1	12	W	756.2		W				753.8		W	$2\nu_5' + \nu_6' - \delta$
782.4	16	W	783.5	18	W	782.9		W	784.8		W	$2\nu_5' + \nu_6'$

TABLE IX *(Continued)*

$\Delta\nu$ (cm^{-1})	FWHH (cm^{-1}) I	$\Delta\nu$ (cm^{-1})	FWHH (cm^{-1}) I	$\Delta\nu$ (cm^{-1})	FWHH (cm^{-1}) I	$\Delta\nu$ (cm^{-1})	FWHH (cm^{-1}) I	Assignment
ReF$_6$/MoF$_6$		ReF$_6$/WF$_6$		ReF$_6$/UF$_6$		ReF$_6$		
				825.9	VW			$\nu_4' + 2\nu_5' - \delta$
838.7	VVW	844.7				842.3	VW	$\nu_5' + \nu_1' - \nu_6'', \nu_5' + 3\nu_6'$
		847.1	W					$\nu_5' + \nu_1' - \nu_6'', \nu_1' + \nu_6' - \delta$
		873.0	W					$\nu_4' \; 2\nu_5'$
873.7	M	877.7	M			867.4		$\nu_1' + \nu_6' - \delta, \nu_4' + 2\nu_5'$
894.4	13 M	895.4	15 M	891.8	20 M	895.1	18 W	$\nu_1' + \nu_6'$
		960.1	W	934.1	W			$\nu_1' + \nu_4' - \delta$
980.3	39 W							
		985.8	W			984.5	34 W	$\nu_1' + \nu_4'$
				980.0	W			$\nu_1' + \nu_4', \nu_1' + \nu_5' - \delta$
		1016.0	VW	1016.9	W	1019.5	VVW	$\nu_1' + \nu_5'$
		1049.9	VW			1056.0	VVW	$\nu_1' + 2\nu_6' - \delta, 3\nu_5' + \nu_6' - \delta$
		1083.0	VW			1088.9	VVW	$\nu_1' + 2\nu_6', 3\nu_5' + \nu_6'$
		1169.8	W	1151.1	VW	1166.7	VW	$\nu_1' + \nu_5' + \nu_6' - \delta$
1173.6	W							$\nu_1' + \nu_5' + \nu_6' - \delta, \nu_4' + 3\nu_5'$
1195.4	W	1196.5	W	1191.0	VW	1196.5	VW	$\nu_1' + \nu_5' + \nu_6'$
		1403.4	VW			1401.9	VW	$2\nu_1' - \delta$
		1434.3	VW	1427.3	W	1431.6	VW	$2\nu_1'$
1585.5	VW	1583.9	W	1560.3	VW	1576.1	VW	$2\nu_1' + \nu_6' - \delta$
1609.5	W	1610.0	W	1603.4	W	1609.6	VW	$2\nu_1' + \nu_6'$
				1689.5	VVW			$2\nu_1' + \nu_4', 2\nu_1' + \nu_5' - \delta$
		1697.7	VVW					$2\nu_1' + \nu_4'$
		1729.7	VVW	1732.5	VVW			$2\nu_1' + \nu_5'$

[a]The observed pure crystal origin is at 4999.7 cm^{-1}, but the vibronic spectra are measured from the exciton band center position found to lie at 5003.7 cm^{-1} as discussed in the text, Sec. VI. E.

[b]Although only ν_1' is listed, ν_3' occurs in this peak and in combination, difference, and overtone peaks (see text).

electronic hot band linewidths (7, 14, and 14 cm^{-1}, respectively) are phonon determined, the same ordering for increasing exciton–photon coupling is found, even though sideband intensity and linewidth may not be directly related through a single coupling mechanism.

An interesting feature in the hot bands is the structure of ν_6'' vibrations. In mixed crystals, the vibration (t_{2u} in O_h) is observed to be split into two components, ν_{6a}'' and ν_{6b}'', separated by approximately 10 cm^{-1}. This structure occurs at $(\nu_0 - \nu_{6a}''), (\nu_0 - \nu_{6b}'')$, and again at $(\nu_0 - \delta - \nu_{6a}''), (\nu_0 - \delta - \nu_{6b}'')$ (see Fig. 9). The ν_6'' vibrations are thus similar in both lower electronic levels and large ν_6'' splitting compared to that for ν_6' (≤ 4 cm^{-1} see Table VIII and Fig. 10) indicates a greater distortion for the lower ReF$_6$ electronic levels. These lower levels are vibronically mixed (Jahn–Teller coupled), while the 5000 cm^{-1} Γ_{7r} level is an energetically isolated electronic Kramers doublet.

To test assignment of the lowest level as $\Gamma_{6g}(D_{4h})$, an attempt was made to compare relative origin transition intensities allowing for population differences in the various crystals. However, appropriately averaged transition matrix elements are the same for both states to within 1% (using parameters listed in Fig. 3). Consequently, no comment may be made on the assignment from the unpolarized absorption spectra.

C. Two-particle transitions

Although locations of major vibronic features in the various crystal spectra are nearly identical relative to their respective origins, there is a great deal of intensity and line shape variation among similarly identified features. [Compare Figs. 6(a), 6(b), 6(c), 6(d).] For example, $(\nu_0 + \nu_6')$ is broad $(\Delta\nu \sim 20$ cm$^{-1})$ and has underlying structure in UF$_6$, is sharp in MoF$_6$ and WF$_6$, and has a shoulder to the red in ReF$_6$. Also, $(\nu_0 + \nu_4')$ is very broad with structure to the red in MoF$_6$, WF$_6$, and ReF$_6$, while it is sharp in UF$_6$. Furthermore, there are medium intensity broad peaks not assignable to vibrations of ReF$_6$ (C_s or O_h or D_{4h}) occurring red of $(\nu_0 + \nu_6')$ and blue of $(\nu_0 + \nu_5')$ in WF$_6$ and MoF$_6$ but not in UF$_6$ or ReF$_6$ crystals.

TABLE X. Two-particle transition data.

ReF$_6$ excited level vibration	Host	Vibron energy[a] (cm^{-1})	Host vibration (ground state)	Two-particle energy[a] (cm^{-1})	Host crystal vibration[b] (cm^{-1})	Fractional vibron intensity ($\lvert a \rvert^2$)	Approximate reduced vibron-two-particle separation[c]
ν_6	MoF$_6$	177.4 180.0	ν_6	135.6 141.0 146.5 152.6	~128 ~140	0.81	1.7
	WF$_6$	177.3 180.6	ν_6	154.6	~147	0.67	1.2
	UF$_6$	175.6 178.8	ν_4	173.3 181.6 185.1 194.5	174.0 183.8 190.2		
			ν_5	202.9 206.2 214.2 219.5	204.9 209.8 213.7 224.2 226.9		
	ReF$_6$	184.4[d]	ν_6	170.7[d]	~167(167[e]) ~180(177[e])		
ν_5	MoF$_6$	302.4 303.8	ν_5	315.1 318.0 320.7	315.1 318.5 323.7	0.69	1.7
	WF$_6$	302.4 304.0	ν_5	320.8 322.2 324.5	320.5 323.2 328.0	0.83	2.7
ν_4	MoF$_6$	270.9 272.4 274.1	ν_4	247.2 251.2 254.0 259.5 262.0 263.7 265.1	246.7 251.4 260.7 271.1	≲0.5	
	WF$_6$	269.0 271.7	ν_4	242.6 251.1 252.3 255.0 256.0 264.8	239.5 249.4 265.1	~0.5	
	ReF$_6$	271.7[d]	ν_4, ν_5		~232 ~258		
ν_1, ν_3[f]	MoF$_6$	~718	ν_2	644.8 650.6	640.9 643.9 650.9		
			ν_3	693.9 696.5	693.9 700.0		
			ν_1	741.6	740.8		
	WF$_6$	~717	ν_1	771.7	771.9		
	UF$_6$	~713	ν_1	664.5	661.8		
$\nu_5 + \nu_6$[g]		~480	ν_2	517.1	509.3 515.2 516.6 532.8		

[a]These energies are tabulated as the difference between the corresponding vibronic and zero-phonon lines in the appropriate crystals.

[b]E. R. Bernstein and G. R. Meredith, "Raman Studies of Crystalline Transition Metal Hexa-fluorides," (in preparation).

[c]Reduced separation equals estimated vibron to two-particle band center energy divided by vibrational exciton bandwidth estimated from observed two-particle transition and Raman data.

[d]Transition energy minus 0–0 total exciton band center energy (see text).

[e]Averaged mixed crystal hot band values (see Table IX).

[f]$(2\nu_5)$, $(\nu_4 + 2\nu_6)$, $(\nu_5 + 2\nu_6)$, and $(2\nu_5 + \nu_6)$ of ReF$_6$ also fall in this general region and most likely also contribute to the overall two-particle intensity.

[g]$(2\nu_4)$, $(3\nu_6)$, $(\nu_4 + \nu_5)$, and $(2\nu_5)$ of ReF$_6$ also fall in this region and most likely also contribute to the overall two-particle intensity.

These absorptions are all attributable to two-particle transitions. A zeroth-order description of a two-particle transition is an optical excitation of the crystal for which the final state has electronic and vibrational quanta located on different sites. The energetics of this explanation are quite convincing, as Table X shows.

As was pointed out in Sec. III, Rashba has developed a theory to explain two-particle transitions in aromatic crystals, in which electronic and vibrational components of a vibronic state are treated as separate interacting particles. The frequency defect $\Delta_\nu = \nu' - \nu''$ acts as a local perturbation or potential for the exciton-vibration interaction. It is the ratio of $|\Delta_\nu|$ to Δ_{ex}, the electronic exciton bandwidth, which determines the proportion $1 - |a|^2$ of total vibron (one-particle) band intensity occurring in the two-particle band.

In attempting to apply the Rashba theory to mixed crystals of ReF_6 in UF_6, MoF_6, and WF_6, two important points should be considered. First, the 2μ transition in ReF_6 is well isolated from the nearest electronic exciton band in any of the mixed crystals; indeed, this separation varies from ~20000 cm^{-1} to ~55000 cm^{-1}. Second, the three mixed crystal spectra and pure crystal spectra are strikingly similar in overall two-particle features. Ignoring pseudoresonance in mixed crystals, any modified Rashba theory would have to reduce to one in which the vibrational exciton band of the host replaced the electronic exciton band and the localized electronic excitation of the guest replaced the localized vibration. The frequency defect then becomes $\Delta_\nu = \nu'_g - \nu''_h$, the vibration frequency difference between the electronically excited guest and the electronic ground state of the host.

Since host ground state vibrations are described as excitons and the presence of impurity molecules must relax $\Delta k = 0$ exciton selection rules, two-particle transitions may have widths comparable to host vibrational

FIG. 11. Fractional vibron (one-particle) intensity ($|a|^2$) as a function of observed vibron location relative to the two-particle band center (ν). Results of calculations based on the modified Rashba model (see text and Ref. 24) are displayed for vibrational exciton densities of states approximated by (a) $\rho(\omega) = \pi/2 \cos(\pi\omega)$, $|\omega| \leq \frac{1}{2}$; (b), (c), (d), $\rho(\omega) = A(\beta) e^{-\beta\omega}$, $|\omega| \leq \frac{1}{2}$, $A(\beta) = [2\int_0^{1/2} e^{-\beta\omega^2} d\omega]^{-1}$; (b) $\beta = 7$; (c) $\beta = 5$; (d) $\beta = 3$; (e) $\rho(\omega) = 1$, $|\omega| \leq \frac{1}{2}$.

exciton bandwidths. In fact, the ν_5 and ν_6 two-particle bands are wider than the single particle peaks in MoF_6 and WF_6 (see Fig. 6). Since ν_4 transforms as the electric dipole in 0_h, D_{4h}, and C_s, it is expected to have the largest exciton bandwidth. The low resolution spectra of the ν'_4 region show considerable broadness in MoF_6 and WF_6 crystals, and the higher resolution spectra display at least five features (see Table X).

The fraction of intensity which occurs in two-particle bands $1 - |a|^2$ and which derives oscillator strength from a single vibronic transition decreases with increasing $|\Delta_\nu|/\Delta_{ex}$, according to the Rashba theory. Table X lists the fractions of single particle vibronic intensity, $|a|^2$, ignoring intensity borrowing from neighboring vibronic bands. A major difficulty which arises with this modified Rashba approach is that it would predict $|a|^2 \simeq 1$ when $|\Delta_\nu| \geq \Delta_{ex}$, a fact which is substantiated in benzene ($\Delta_\nu = -86$ cm^{-1} and $\Delta_{ex} = 60$ cm^{-1} predicts $|a|^2 = 0.98$, and $|a|^2 = 0.95$ was observed).[24a] The ReF_6 values for $|a|^2$ are significantly lower than predicted, implying that too much vibron intensity resides in the two-particle states. Disregarding additional complexity arising from other nearby bands, it appears that the interaction of optically allowed one-particle vibron states with the multitude of two-particle separated configuration states cannot be quantitatively described in terms of just Δ_ν and Δ_{ex} parameters. Figure 11 depicts calculations of $|a|^2$ based on a square wave, sine wave $(0°-180°)$, and Gaussian distribution of exciton density of states for comparison.

One would initially expect that this theory, which omits corrections for resonance interactions and renormalized energies, would be a better approximation for the present case of host vibrational exciton bands with small Δ_{ex} than it appears to be for the case of electronic exciton bands with large Δ_{ex}. The superexchange mechanism (interaction through a higher electronic exciton band—see Sec. VI. D) is seen to be of little help in improving this approach because of the similar magnitude of the effects in the various mixed and pure crystals.

It is well known that an impurity level lying outside a band with which it interacts is repelled from the band edge. Positions of single-particle transitions observed in absorption are consequently not necessarily situated at a distance ν' from the origin or electronic band center. High resolution data show that the ν'_5 optical centers of gravity predict host independent vibrational centers of gravity (Table XI). However, the ν'_4 modes in mixed crystals differ by 3–4 cm^{-1}, with the highest value of ν'_4 being associated with the smallest $|\Delta_\nu|$ system. The percentage of ν_4 two-particle transition intensity is large in MoF_6 and WF_6 but very small in UF_6. Consequently, the unperturbed ν'_4 frequency is most probably the value observed in UF_6 mixed crystals. Likewise, the ν'_6 centers of gravity are very close in MoF_6 and WF_6, but ν'_6 in UF_6 is shifted to lower energy by ν''_4 and ν''_5 two-particle bands.

The above modified Rashba theory is of course not applicable to the pure crystal case. The electronic exciton structure, which is at present incompletely
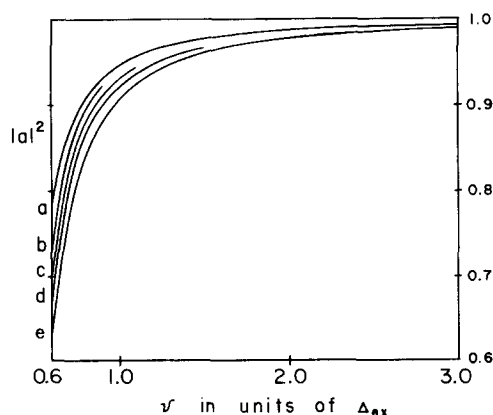
TABLE XI. Vibrational centers of gravity from high resolution spectra.

ReF_6 vibration	In MoF_6	In WF_6	In UF_6
ν_6	179.6	179.5	176.7
ν_4	272.5	269.9	265.8
ν_5	302.9	302.9	302.9
ν_1			712.9
	718.2[a]	716.7[a]	
ν_3			715.5

[a]In this host, the ν_1/ν_3 region connot be assigned to specific resolved features.

understood, must be included. Vibronic coupling for non-totally-symmetric vibrations might also be expected to contribute. Nonetheless, it should be noted that pure crystal two-particle energies and intensities are not significantly different from those of mixed crystals. This observation tends to eliminate higher order or superexchange-type mixing with delocalized charge transfer exciton bands, as well as the electronic exciton band of the $\Gamma_{7g}(D_{4h})$ electronic state itself, as major sources of two-particle intensity. A rather straightforward first-order mixing of one- and two-particle states via the intermolecular potential seems to be indicated.

Two-particle related quantitative data are difficult to obtain from pure crystal absorption spectra. The ν_4 and ν_5 two-particle transitions occur within the broad envelop of the ν_4' vibronic peak. The ν_6 two-particle transitions are observable as an unresolved shoulder of the ν_6' one-particle vibronic peak (see Fig. 6).

Two-particle features are also indentified in combination and overtone vibronic transitions (Table VIII). Distinctive shapes of ν_4 two-particle transitions in WF_6 and MoF_6 and of ν_6 in UF_6 make their assignment particularly simple in the $(\nu_4' + \nu_5')$ and $2\nu_6'$ regions. This structure suggests transfer of only one vibrational

quantum to the host. Transitions to states in which more than one vibrational quantum is transferred were not observed.

D. Pair spectra in mixed crystals

To aid in the decomposition of interactions involved in the pure crystal origin structure, pair or dimer ReF_6 spectra have been investigated in dilute mixed crystals. Such studies could be performed with relative ease because dilute crystal origins are quite sharp. At 0.3% ReF_6 concentration, the full-widths at half-height (FWHH) for MoF_6, WF_6, and UF_6 crystals were 0.7, 0.9, and 1.1 cm^{-1}, respectively. The increasing trend in these numbers probably indicates lower concentrations would yield sharper lines. For some of the well resolved pair features in UF_6, a 0.5 cm^{-1} FWHH was measured. This latter width is of the order of the zero-field hyperfine structure for the transition, and thus is most likely intrinsic.

As pointed out previously, the four crystal systems involved in the study (ReF_6, WF_6, MoF_6, and UF_6) are nearly identical. The potentials experienced by ReF_6 guests in the various hosts (including the paramagnetic pure crystal) are all similar in that the 0–0 transitions are all within 20 cm^{-1} of one another. (See Table XII). When their transition energies are modified to account for the lower symmetry crystal splitting of the Γ_{8g} octahedral ground state by normalizing to the ReF_6 pure crystal splitting, these differences fall within 6 cm^{-1}, as shown in Table XII. The monomeric ReF_6 infinite dilution wavefunctions are expected to be interchangeable between hosts; replacement of a neighboring host molecule by a ReF_6 molecule is expected to have small effect on the original ReF_6 site wavefunctions and energies.

Pair structure, determined by the variation of intensity as a function of guest concentration, has been observed around the origin in all three host crystals. Figure 12 illustrates such structure in MoF_6 and UF_6
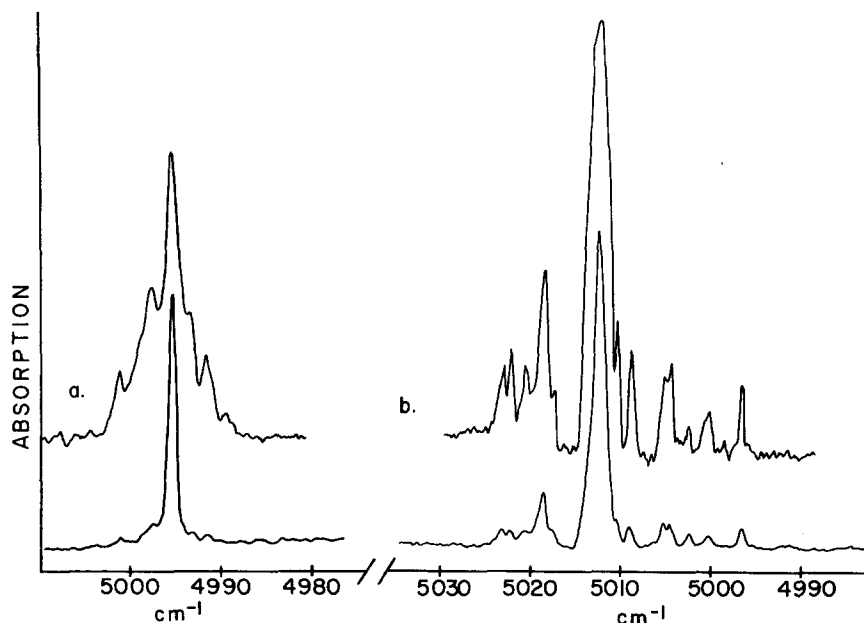

FIG. 12. Absorption spectra displaying dimer structure in the origin region. (a) ReF_6 in MoF_6. The upper trace is 2% ReF_6 and the lower trace is 0.3% ReF_6. Slitwidths are ~0.5 cm^{-1}; (b) ReF_6 in UF_6. The upper trace is 0.8% ReF_6 and the lower trace is 0.3% ReF_6. Slitwidths are 0.3 and 0.6 cm^{-1}, respectively. Note that some of the dimer lines in UF_6 are roughly 0.5 cm^{-1} FWHH.

TABLE XII. Energies of ReF_6 electronic transitions in various crystals. ν_0 is the observed low temperature origin. δ is the ground state splitting as determined from hot bands. $\bar{\nu} = \nu_0 + (\delta_{ReF_6} - \delta_{MF_6})/2$ is a normalization to the neat ReF_6 crystal ground state splitting.

Host	ν_0(cm^{-1})	δ(cm^{-1})	$\bar{\nu}$(cm^{-1})
MoF_6	4995.4	23.1	4997.3
WF_6	5000.0	24.6	5001.0
UF_6	5012.5	45.9	5002.9
ReF_6(77 K)	5003.7[a]	26.8	5003.7

[a]Vibronic extrapolated origin. See text.

mixed crystals; the over-all extent of the structure is ~ 12 cm^{-1} in MoF_6 and WF_6 but ~ 27 cm^{-1} in UF_6. Since there are six inequivalent types of nearest neighbor pairs and both ground and excited state interactions are possible, this spread is not necessarily directly related to the magnitude of interaction in a given dimer. Nonetheless, structure in the hosts is centered roughly about the monomer line, and since the gas-to-crystal shift is not expected to differ much for a pair from that of a monomer, the splitting is an *indication* of the magnitude of dimer interactions. Selection rules play a very minor role in this low symmetry, strongly spin-orbit coupled situation.

One might initially expect that most of the pair features would occur on the high energy side of the monomer origin due to ground state interactions. However, any two ReF_6 molecules can couple ferro-, antiferro-, or canted antiferromagnetically in either ground or excited state. Each pair has its own particular structure, and more than one level of the ground dimer may have population at a given sample temperature. Where the pair features are reasonably well resolved, structure to the high-energy side of the monomer is most intense. Careful intensity vs temperature studies have been hampered by line broadening and overlapping in this crowded region.

The only substantial difference between the ReF_6/UF_6 and ReF_6/MoF_6, WF_6 systems that could account for these interaction differences is found in the positions of the host charge transfer bands. Charge transfer bands of MoF_6 and WF_6 are quite high in energy (at and above 50 000 cm^{-1} and 60 000 cm^{-1}, respectively),[3f] while those of ReF_6 and UF_6 fall around 23 000 cm^{-1}. The overlapping charge transfer bands for the ReF_6/UF_6 mixed crystal around 23 000 cm^{-1} and above allow for delocalization of these low energy ReF_6 states in UF_6 mixed crystal (and pure ReF_6 as well; see Sec. VI. E). In the energy region of this charge transfer exciton band, the ReF_6/UF_6 mixed crystal would be virtually identical to the ReF_6 pure crystal. Additionally, the first ionization potentials[3f,h] and charge transfer energies predict the lowest empty orbitals of ReF_6 and UF_6 to be 3.5 eV lower than the lowest empty orbital of WF_6. Intersite electron mobility and second order interactions ("kinetic exchange" or "superexchange") between guests are substantially enhanced in UF_6 and ReF_6 crystal. Such low lying delocalized

states would not occur in ReF_6/MoF_6, WF_6 mixed crystals. There appears to be an intermolecular superexchange mechanism, which increases the interaction between two ReF_6 molecules in their ground and first excited states; the pathway for such interaction is associated with the delocalized (exciton) charge transfer band of the host and intersite electron mobility. Pair interactions observed in MoF_6 and WF_6 mixed crystals should yield an effective upper limit to the more usual molecular crystal exciton (energy transfer or excitation exchange) first-order pair interactions.

It would be useful to separate the total origin pair interactions into the "usual" *exciton* (resonance or excitation exchange) and *electron exchange* terms. Such a decomposition would be straight forward for a pure Heisenberg exchange interaction [with $\xi(\mathbf{L} \cdot \mathbf{S}) = 0$]; this reduction would also lead to a spin-orthogonal singlet-triplet coupling regime in both ground and excited states. In the present situation there are diagonal and off-diagonal exchange terms within each state, excitation exchange terms in the excited state, and terms that couple the two states. A detailed consideration of the matrix elements involved reveals that excitation and electron exchange distinctions are not, in general, possible, owing to the strong coupling of internal and orbital electron coordinates.

On the other hand, having identified the major intersite interaction mechanism as superexchange via low lying delocalized charge transfer exciton bands, it is possible to further decompose the over-all intermolecular coupling. In particular, one can conveniently employ the localized product representation $a |\chi^f \chi^0\rangle$ or $|\Gamma_3 \Gamma_4\rangle$ and assume all $\langle \Gamma_3^f \Gamma_4 | \mathcal{K}' | \Gamma_4 \Gamma_3 \rangle$, which are off diagonal with respect to the zeroth-order degenerate ground and excited state blocks, are zero. In this approximate simplification of the total interaction there are three types of terms: diagonal-(degenerate)-block ground state matrix elements (e.g., $\langle \Gamma_3 \Gamma_4 | \mathcal{K}' | \Gamma_4 \Gamma_3 \rangle$), diagonal-(degenerate)-block excited state matrix elements which localize the excitation (e.g., $\langle \Gamma_3^f \Gamma_4 | \mathcal{K}' | \Gamma_4^f \Gamma_3 \rangle$), and off-diagonal excited state matrix elements which exchange or delocalize excitation (e.g., $\langle \Gamma_3^f \Gamma_4 | \mathcal{K}' | \Gamma_4 \Gamma_3^f \rangle$). The off-diagonal excited state terms are still, of course, within the zeroth-order degenerate excited state "diagonal" block. These latter terms are subject to reduction by vibrational overlap factors. For non-totally-symmetric vibronic states of the monomer, excitation exchange terms are zero in the Born-Oppenheimer 0_h symmetry approximation. They are expected to be small for vibronic states of ReF_6, except, perhaps, in ν_5, for which the ground state functions are not Born-Oppenheimer in nature.

In UF_6, pair peaks occur around ν_4' and ν_5' with spreads of ~ 25 and 20 cm^{-1} (see Fig. 13), respectively. In WF_6 and MoF_6 hosts, the monomer peaks for ν_4' and ν_5' also appear to change with concentration, and poorly resolved structure occurs on these features ($\Delta\nu < 10$ cm^{-1}). Intensity difficulties, two-particle transitions, congestion, and assignment uncertainties prevent adequate characterizations of dimer features near other vibronic transitions. These data indicate that the
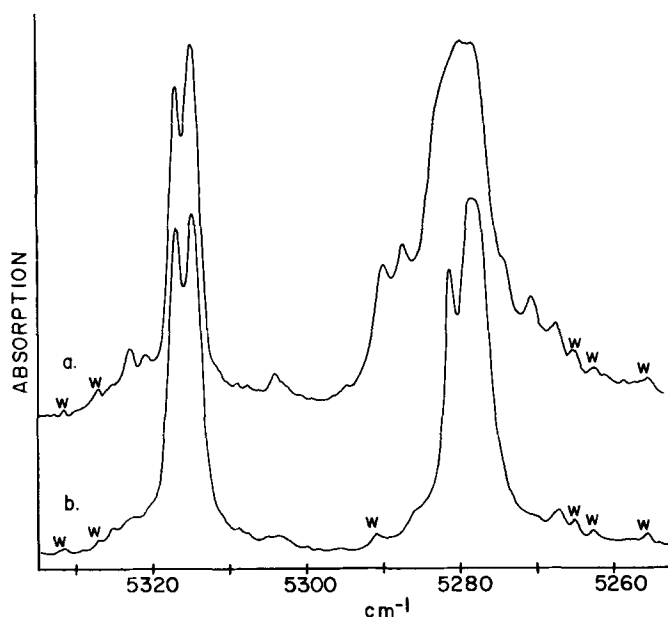
FIG. 13. Absorption spectra displaying dimer structure in the ν_4', ν_5' region of ReF_6 in UF_6. (a) is 0.8% ReF_6; (b) is 0.3% ReF_6. Slitwidths are ~0.5 cm^{-1}.

diagonal energy localizing ("exchange") interactions are large.

The excited state pair wise exchange splittings should be reduced in the pure crystal (by roughly a factor of 2) with respect to those in ReF_6 pairs in UF_6, because the ordered pure crystal ground state is nondegenerate. The reduction can be seen qualitatively as due to the restricted spin orientation for an ordered pure crystal ground state. The total interaction, which is approximately a sum over all pair terms, should still be observed if the major contribution came from excited state matrix elements. The pure crystal exchange field would then split the localized Kramers doublet vibronic states by an observable amount. Selection rules for C_s site (exchange field) symmetry give intensity to both terms of the split Kramers doublet. Approximate D_{4h}-site symmetry leads to the same result for arbitrary orientation of axes. However, pure crystal (2 K) spectra show ν_1'/ν_3' and ν_5' to be as sharp as mixed crystal peaks, and there is no evidence of splitting. Since this splitting or broadening should be observed if the major contribution to the pair splittings were an excited state effect, it is possible to argue that large block diagonal interactions for pairs are most likely in the ground state.

Based on the above supposition, pair interactions are qualitatively proportional to the over-all energy spread of the origin structure [$\delta\nu$ (ReF_6/UF_6) ~27 cm^{-1} and $\delta\nu$ (ReF_6/MoF_6, WF_6) ~12 cm^{-1}]. Using an energy denominator argument, the ratio of ground state superexchange interaction in ReF_6/UF_6 to ReF_6/WF_6, MoF_6 is roughly $2\frac{1}{2}:1$. If excitation exchange interactions are constant through the series, one finds that splitting due to superexchange appears to be the major contribution to the origin structure in all mixed crystals.

It would of course be important to actually deter-

mine these decompositions experimentally. Essential experiments to unravel pair interaction involve single oriented crystals, polarized light, the Zeeman effect, and temperature dependent absorption. These are presently under investigation in our laboratory.

E. Pure crystal origin

Transition energies to various levels of ReF_6 in mixed crystals are temperature independent to within the measurement uncertainties as determined from low resolution spectra at 77 and 2 K (see Table VIII and IX). Either there is relatively low sensitivity of the general vibrational force field and electronic energy level spacings of ReF_6 to changes in lattice constant, or there is negligible lattice change over this temperature range for UF_6, MoF_6, and WF_6 crystals. However, pure crystal vibronic transitions are generally blue shifted by ~6 cm^{-1} on cooling from 77 to 2 K (bath $T \approx 1.5$ K). Since XF_6 crystals are so nearly identical, this indicates the onset of a pure crystal cooperative phenomenon such as a structural phase change or magnetic ordering. The former might be related to Jahn–Teller activity of ReF_6 or to depopulation of the Γ_{7g} (D_{4h}) level at 30 cm^{-1}. A structural change can be eliminated, however, by the careful heat capacity studies of Weinstock et al.[31] Magnetic susceptibility measurements (see below, Sec. VI. F) show that, in fact, a magnetic transition probably occurs somewhat below 1.5 K.

The pure crystal origin evidences some striking difference between 77 and 2 K, as shown in Fig. 14. The three most pertinent temperature effects are (1) a decrease in width with increasing temperature [$\delta\nu$ (2 K) ~40 cm^{-1} and $\delta\nu$ (77 K) ~25 cm^{-1}]—considerations of exciton–phonon coupling and population of the 30 cm^{-1} Γ_{7g} (D_{4h}) excited state would lead to the opposite effect; (2) several features are evident in the 1.5 K spectra which appear to be, from their intensity and position, k = 0 components of the same exciton band. The 4.2 K spectra are more poorly resolved but have the same over-all width and features; and (3) a change in observed band center of +6 cm^{-1} on cooling from 77 K to 2 K. All of these features can be readily understood based on a low temperature magnetic phase transition or the dominance of exchange interactions below 4 K in the pure crystal.

In order to discuss the 0–0 band in detail, it is necessary to understand what parts of it are observed and where its center lies. Various group theoretical considerations and selection rules based on magnetic space groups were presented in Sec. III. Magnetic space group analysis may still be central to this discussion even if the pure crystal is not yet ordered at 1.5 K (see Sec. VI. F). Local order or short-range exchange induced correlations (brought about by large anisotropic exchange fields) may well be dominant as high as 4–5 K. Assuming k is still approximately a good quantum number under these circumstances, the observed center of gravity of the k = 0 optical components will in general be shifted from the total band center by a "k = 0 shift"[11] and by variations in the transition moment to different Davydov components. Since non-totally-

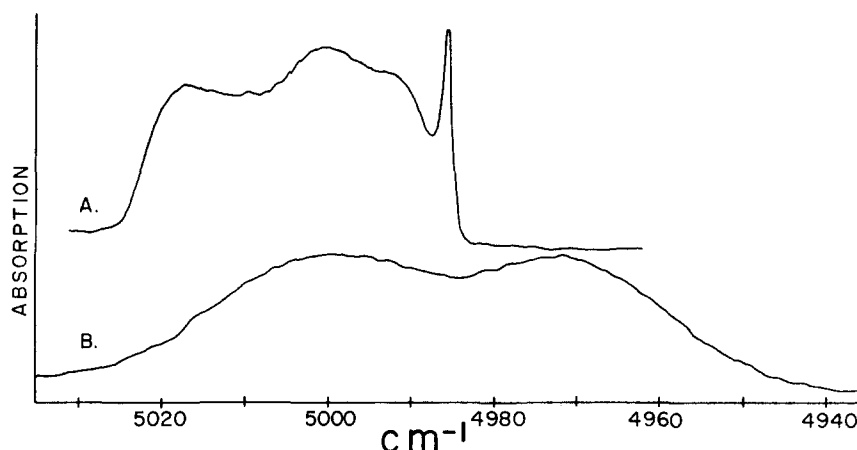ABSORPTION

A.

B.

5020   5000   4980   4960   4940

cm⁻¹

FIG. 14. Absorption spectra of the origin of ReF₆ neat crystals, (a) is near 2 K; (b) is near 77 K. Even though polarized spectra have not been obtained, the sharp feature at 4986 cm⁻¹ in the 2 K spectrum has been found to be polarization dependent in one favorably oriented single crystal sample.

symmetric vibron (single particle) dispersion and Davydov splitting are reduced by intermolecular vibrational overlap factors and these features are sharp (all exchange field split components are expected to be of comparable intensity for unpolarized light and randomly oriented single crystals in either a C_s or D_{4h} site model), the observed vibron band centers must lie close to their $k=0$ and total exciton band centers. Employing host-independent values of ν_1'/ν_3', ν_5' and ν_6' fundamentals (Table XI), the 0–0 total exciton band centers at 2 K and 77 K can be extrapolated from the vibron absorption band centers. These values are 5009.5 (1.2) cm⁻¹ (2 K) and 5003.7 (1.0) cm⁻¹ (77 K); the observed absorption band centers lie at 5005.1 (0.25) cm⁻¹ and 4999.7 (0.30) cm⁻¹, respectively. The difference between the vibronic extrapolated band center and the observed band center at 77 K is expected from general considerations of exciton–phonon coupling. The 4.4 cm⁻¹ difference between extrapolated and observed band centers at 2 K encompasses effects from both $k=0$ shift terms and unobserved exciton branches.

Corrected values for the mixed crystals origins can also be compared to various measures of the band center. These values, given by $\bar{\nu} = \nu_0 + (\delta_{ReF_6} - \delta)/2$ (see Sec. VI. B and Table XII) are $\bar{\nu}$ (Re/Mo) = 4997.3 cm⁻¹, $\bar{\nu}$ (Re/W) = 5001.0 cm⁻¹, and $\bar{\nu}$ (Re/U) = 5002.9 cm⁻¹. Simple exciton theory for molecular crystals would predict that mixed crystal origins should be close to the total band center. In the ordered crystal, the ground state is lowered by 5.8 cm⁻¹ [with respect to the 5000 cm⁻¹ Γ_{7_g} (D_{4h}) level] as reflected in the increased absolute energy of the entire vibronic manifold. It is the 77 K paramagnetic crystal band center that should be compared to an ("ideal") mixed crystal value for the band center. Standard host–guest quasiresonance corrections would not be necessary in this instance. Probably the best mixed crystal value to choose for this comparison is $\bar{\nu}$ (Re/U) = 5002.9 cm⁻¹ because of the similarity between ReF₆ pure and ReF₆/UF₆ mixed crystals. Thus the 77 K vibronic origin (5003.7 cm⁻¹) and the ideal mixed crystal origin (ReF₆/UF₆ at 5002.9 cm⁻¹), coincide to within ±1 cm⁻¹.

The gas phase origins have been reported as 5001 cm⁻¹ [3c] and 4993 cm⁻¹ [3b]; the latter value is based on somewhat higher resolution data, but the major differ-

ence between the two numbers is interpretational in nature. The gas-to-crystal shift is small, but its exact value cannot be presently determined from published data.

Two alternative explanations for the ReF₆ pure crystal origin structure at low temperature are possible.

1. Structure is due to transitions to the large number of $k=0$ components of the Davydov branches for the appropriate magnetic space group (Sec. III). Since the crystal may not actually be ordered at 1.5 K, the "exciton band" would be indicative of short-range (unit cell) order, and k would only be an approximate quantum number. $\Delta k=0$ selection rules would be a first-order approximation for the discussion of band shape, etc. The interaction would be a large excitation exchange (off diagonal in the excited state "diagonal block"), apparently larger than in the dimers. However, the total band is composed of sums of dimer interaction terms. A peculiarity of this interpretation is that the translationally equivalent interactions ($k=0$ shift), which are expected to be large, would have to cancel in part because the optically observed band center and the total (vibronically predicted) band center are close.

2. The structure is due in part to magnon-type spin fluctuations. These spin fluctuations appear as magnon side bands obeying total $\Delta k=0$ selection rule. The observed structure would contain both magnon and exciton states. This interpretation is appealing because it is consistent with large diagonal ground state interactions and because it offers an explanation for the significantly increased intensity in the origin of the "ordered" crystal relative to that in the mixed or paramagnetic crystal. The sharp orientation (polarization) dependent feature on the red edge of the band would be an allowed $k=0$ Davydov component occurring at the bottom of the exciton band. Other higher-energy Davydov components may be broadened owing to the magnon sideband continuum, making them unobservable without careful polarization studies. However, location of the total band center a few cm⁻¹ higher than the optical band center requires that transition probabilities to lower energy exciton plus magnon states dominate the band structure.

Unfortunately, these two possible explanations, both of which seem to have small difficulties, can account for the general observations. Section III discusses the expected magnetic space groups if D_{2h}^{16} is still maintained for the spatial arrangement of molecules. An unambiguous interpretation is not possible at present. Stark, Zeeman, polarization, and better temperature variation experiments are needed in all crystal systems to parametrize both the pair and the exciton band features. It would be extremely informative to attempt a synthesis of the exciton structure from identified pair interactions. Such a relationship exists for diamagnetic molecular crystals and would be important to test for this situation as well.

F. Magnetic susceptibility

The magnetic susceptibility measured between 300 and 10 K is linearly dependent on $1/T$ with a slope of 69 $\times 10^{-4}$ emu-deg/mole. Deviations from this line at lower temperature will be discussed below. The effective moment μ_{eff} is 0.272 for a spin doublet. No deviations in the data were observed for the temperature range corresponding to 30 cm^{-1}, verifying the nearly identical $|\bar{g}|$ values calculated in a D_{4h} model for low lying Γ_{7g} and Γ_{6g} levels.

The observed $|\bar{g}|$ value is significantly lower than that calculated with $k = 1$ ($|\bar{g}| = 0.349$). If k is reduced, $|\bar{g}|$ increases and thus a simple description of ReF$_6$ magnetic properties based on d orbitals and a single orbital reduction factor appears to be inadequate. The spin–orbit operator in t_{2g} orbitals was written as $\xi \mathbf{l} \cdot \mathbf{s}$ and ξ was subsequently determined from intraconfigurational transitions between strong field 5d hexafluoride states.[1,3] This operator should be written as ξ' $(k_{\tau\tau} \mathbf{l}) \cdot \mathbf{s}$ within a manifold of t_{2g} orbitals. The observed magnetic moment is induced by spin–orbit coupling between t_{2g} and e_g orbitals and should be generated by ξ' $(k_{\sigma\tau} \mathbf{l}) \cdot \mathbf{s}$. When $k_{\sigma\tau} = k_{\tau\tau}$, no error ensues from explicitly dropping k's inherent in the experimental ξ. Since, however, σ bonding is more effective than π bonding, $k_{\sigma\tau} < k_{\tau\tau}$, and induced moments in the lower bands would be expected to be smaller than for the case $k_{\tau\tau} = k_{\sigma\tau}$.

An independent estimate of $k_{\tau\tau}$ can be obtained from Zeeman splitting of the $\Gamma_{7g}(D_{4h})$ level deriving from the $\Gamma_{7g}(0_h)$ level. The calculated g value is isotropic in 0_h and nearly isotropic (within 1 to 2%) in D_{4h}. It is approximately independent of $k_{\sigma\tau}$ and $k_{\sigma\sigma}$ and decreases from $g = 2.00$ at $k_{\tau\tau} = 1$ to $g = 1.33$ at $k_{\tau\tau} = 0.5$. When g is directly determined from experiments it will be possible to comment further on $k_{\tau\tau}$, $k_{\sigma\tau}$ and what can be learned about M–F bonding character from orbital reduction factor–magnetic susceptibility calculations.

For the temperature range 10 K $\geq T \geq 1.5$ K, the magnetic susceptibility is not a linear function of $1/T$. The actual dependence over this range is quite complex and at best only qualitatively understood. While the high temperature data give a small antiferromagnetic Weiss constant ($\theta \approx 0.5$ K), the lower temperature results ($T \leq 7$ K) appear to give ferromagnetic behavior. The exchange interaction is very anisotropic. It appears as

though the pure solid has not ordered at $T = 1.5$ K, although exchange interactions are dominant below about 4 K. The measured susceptibility is consistent with lower than three-dimensional behavior[32] and both ferro- and antiferromagnetic interactions with nearest neighbor molecules.

VII. CONCLUSIONS

The major conclusions to be drawn from this work are as follows:

(a) ReF$_6$ crystal spectra are closely related to those of the molecule. The origin is weakly dipole allowed ($E1$ and $M1$), and strong vibronic features serve as false origins forming a number of progressions. For the most part, the excited state potential is quite harmonic, even in the Jahn–Teller active ν_5 mode.

(b) The molecule is octahedral in the gas phase but approximately D_{4h} distorted in the crystal. The ground state $\Gamma_{8g}(0_h)$ is split by 20–50 cm^{-1} (depending on host crystal) owing to this distortion. The ground state potential seems to be more distorted than the excited state (based on ν_6'' site splitting vs ν_6' site splitting). This is probably attributable to a Jahn–Teller effect. However, only ν_5' appears in the excited state (not ν_2'). ν_5' intensity is altered, especially in the pure crystal, by vibronic coupling and two-particle transitions.

(c) The ν_1' and ν_3' region (715 cm^{-1}) of the spectrum has been reassessed and ν_1' and ν_3' are assigned as degenerate.

(d) Pure crystal spectra below about 10 K are dominated by magnetic effects. The susceptibility is complex, anisotropic, and indicative of a balancing of ferro- and antiferromagnetic interactions and reduced dimensionality. The ordering temperature is probably below 1.6 K. An analysis of possible magnetic space groups has been made, and based on the high temperature atomic positions (D_{2h}^{16}-$Pmna$), all types of magnetic arrays are allowed. Selection rules indicate as many as eight k $= 0$ components can be observed in an ordered structure based on D_{2h}^{16} atomic positions.

(e) Pair spectra are observed in the various mixed crystals. The interactions are argued to be largely superexchange dominated the pathway being based on low lying delocalized charge transfer bands in ReF$_6$/UF$_6$ and ReF$_6$. Vibronic spectra indicate energy localizing interactions ("electron exchange") are the most important and that they are probably largest in the ground state.

(f) A great deal of the total vibronic intensity (as much as 25%) resides in two-particle transitions, such that the guest is electronically excited and the host is vibrationally excited. The effect seems roughly constant through the series ReF$_6$/ReF$_6$, ReF$_6$/UF$_6$, ReF$_6$/WF$_6$, and ReF$_6$/MoF$_6$. Mechanisms for this intensity have been evaluated, and one can conclude that a direct mixing between nearly degenerate vibron and two-particle states, through the intermolecular potential, is the dominant intensity source.

(g) Linewidths observed for mixed crystal origins and

pair structure are roughly 0.5 cm^{-1}. This width is within a factor of 2 of the expected hyperfine structure for the transition. Such sharp features imply excellent crystal quality and afford an opportunity to study linewidth and relaxation mechanisms in molecular solids.

In order to obtain more detailed knowledge concerning pure and mixed crystal interactions, Zeeman, Stark, and polarized spectra are needed.

In addition to the research presented in this report, we are also investigating optical and magnetic properties of IrF_6 pure and mixed crystals. Many of the phenomena observed for ReF_6 (magnetic ordering, pair spectra, two-particle transitions, vibronic coupling, crystal field effects, etc.) have been characterized for IrF_6.[12c] This has strengthened and corroborated many of our conclusions and approximations in the present work.

ACKNOWLEDGMENTS

*This research was supported by the NSF, ARO-D, and ONR.

†A preliminary report of this research was presented at the 28th Ohio State Molecular Spectroscopy Conference (June 9–14, 1974; paper number TD 5).

‡Present address: Department of Chemistry, Colorado State University, Port Collins, CO 80523.

[1]W. Moffitt, G. L. Goodman, M. Fred, and B. Weinstock, Mol. Phys. 2, 109 (1959).

[2](a) B. Weinstock and G. L. Goodman, Adv. Chem. Phys. 9, 169 (1965); (b) R. S. McDowell, L. B. Asprey, and R. T. Paine, J. Chem. Phys. 61, 3571 (1974); J. Chem. Phys. 62, 3974 (1975); (c) H. H. Claassen, G. L. Goodman, J. H. Holloway, and H. Selig, J. Chem. Phys. 53, 341 (1970).

[3](a) I. W. Levin, S. Abramowitz, and A. Müller, J. Mol. Spectrosc. 41, 415 (1972); (b) R. McDiarmid, J. Mol. Spectrosc. 38, 495 (1971); (c) J. C. D. Brand, G. L. Goodman, and B. Weinstock, J. Mol. Spectrosc. 38, 449 (1971); (d) J. C. D. Brand and G. L. Goodman, Can. J. Phys. 46, 1721 (1968); (e) J. C. D. Brand, G. L. Goodman, and B. Weinstock, J. Mol. Spectrosc. 37, 464 (1971); (f) R. McDiarmid, J. Mol. Spectrosc. 39, 332 (1971); J. Chem. Phys. 61, 3333 (1974); (g) H. J. Hurst and P. W. Wilson, Spectrosc. Lett. 5, 275 (1972); (h) A. W. Potts, H. J. Lempka, D. G. Streets and W. C. Price, Philos. Trans. R. Soc. London Ser. A 268, 59 (1970).

[4](a) J. C. Eisenstein, J. Chem. Phys. 34, 310 (1961) and references to older work cited therein; (b) H. Selig, F. A. Cafasso, D. M. Gruen, and J. G. Malm, J. Chem. Phys. 36, 3440 (1962).

[5](a) A. Rosén and D. E. Ellis, Chem. Phys. Lett. 27, 595 (1974); J. Chem. Phys. 62, 3039 (1975); (b) J. T. Waber and F. W. Averill, J. Chem. Phys. 60, 4466 (1974).

[6]See, for example, S. Sugano, Y. Tanabe, and H. Kamimura, Multiplets of Transition Metal Ions in Crystals (Academic, New York, 1970).

[7](a) A. A. Kiseljov, J. Phys. B 2, 270 (1969); (b) M. S. Child

and A. C. Roach, Mol. Phys. 9, 281 (1965).

[8](a) R. Englman, The Jahn-Teller Effects in Molecules and Crystals (Wiley-Interscience, New York, 1972); (b) F. S. Ham, in Electron Paramagnetic Resonance, edited by S. Geschwind (Plenum, New York, 1972), p. 1.

[9]E. R. Bernstein and J. D. Webb (unpublished results).

[10]B. Weinstock, Rec. Chem. Prog. 23, 23 (1962).

[11](a) A. S. Davydov, Theory of Molecular Excitons (Plenum, New York, 1971); Usp. Fiz. Nauk 82, 393 (1964) [Sov. Phys.-Usp. 7, 145 (1964)]; (b) G. W. Robinson, Ann. Rev. Phys. Chem. 21, 429 (1970); E. R. Bernstein, S. D. Colson, R. Kopelman, and G. W. Robinson, J. Chem. Phys. 48, 5596 (1968); (c) S. A. Rice and J. Jortner, in Physics and Chemistry of the Organic Solid State, edited by D. Fox, M. M. Labes, and A. Weissberger (Wiley, New York, 1967), Vol. III, p. 199.

[12](a) C. A. Hutchison Jr. and B. Wienstock, J. Chem. Phys. 32, 56 (1960); (b) E. R. Bernstein and G. R. Meredith (unpublished results on ReF_6); (c) E. R. Bernstein and J. D. Webb (unpublished results on IrF_6).

[13](a) E. B. Wilson, J. C. Decius, and P. C. Cross, Molecular Vibrations (McGraw-Hill, New York, 1955); (b) G. Herzberg, Infrared and Raman Spectra of Polyatomic Molecules (Van Nostrand, New York, 1945).

[14](a) J. L. Hoard and J. D. Stroupe, in Chemistry of Uranium, edited by J. J. Katz and E. Rabinowitch (USAEC Commission Washington DC, 1958), Paper 45, p. 325. (b) S. Siegel and D. A. Northrop, Inorg. Chem. 5, 2187 (1966); (c) J. C. Taylor, P. W. Wilson, and J. W. Kelly, Acta Crystallogr. Sect. B 29, 7 (1973); J. H. Levy, J. C. Taylor, and P. W. Wilson, Acta Crystallogr. Sect. B 31, 398 (1975); J. H. Levy, P. L. Sanger, J. C. Taylor, and P. W. Wilson, Acta Crystallogr. Sect. B 31, 1065 (1975).

[15](a) P. Rigny and J. Virlet, J. Chem. Phys. 51, 3807 (1969); Chem. Phys. Lett. 4, 501 (1970); (b) R. Blinc, V. Marenkovic, E. Pirkmajer, I. Zupancic, and S. Maricic, J. Chem. Phys. 38, 2474 (1963); (c) R. Blinc, E. Pirkmajer, J. Slivnik, and I. Zupancic, J. Chem. Phys. 45, 1488 (1966).

[16]A. Abragam and B. Bleaney, Electron Paramagnetic Resonance of Transition Ions (Oxford U.P., Oxford, 1970).

[17]E. Wigner, Group Theory and its Application to Quantum Mechanics of Atomic Spectra (Academic, New York, 1959), Chap. 26.

[18]S. D. Colson, R. Kopelman, and G. W. Robinson, J. Chem. Phys. 47, 27, 5462 (1967).

[19]R. Loudon, Adv. Phys. 17, 243 (1968).

[20](a) W. Opechowski and R. Guccione in Magnetism Vol. II A, edited by G. T. Rado and H. Suhl (Academic, New York, 1965), p. 105; (b) J. O. Demmock and R. G. Wheeler, Phys. Rev. 127, 391 (1962); Mathematics of Physics and Chemistry, edited by H. Margeneau and G. M. Murphy, (Van Nostrand, New York, 1969), Vol. II, Chap. 12; (c) C. J. Bradley and B. L. Davies, Rev. Mod. Phys. 40, 359 (1968).

[21]V. A. Koptsik, Shubnikov Groups (Moscow U.P., Moscow, 1966).

[22]R. M. Hochstrasser and P. N. Prasad, in Excited States, edited by E. C. Lim (Academic, New York, 1974), Vol. I, p. 79.

[23](a) S. Freeman and J. J. Hopfield, Phys. Rev. Lett. 21, 910 (1968); (b) R. S. Meltzer and D. S. McClure, Phys. Rev. 180, 561 (1969).

[24](a) E. F. Sheka, Usp. Fiz. Nauk 104, 593 (1971) [Sov. Phys.-Usp. 14, 484 (1972)]; Physics of Impurity Centers in Crystals, edited by G. S. Zavt (Tallinn, USSR, 1972), p. 431; (b) E. I. Rashba, Physics of Impurity Centers in Crystals, edited by G. S. Zavt (Tallinn, USSR, 1972), p. 417; Y. B. Levinson and E. I. Rashba, Rep. Prog. Phys. 36, 1499 (1973); (c) F. W. Ochs, P. N. Prasad, and R. Kopelman, Chem. Phys. 6, 253 (1974).

[25]D. L. Dexter, Phys. Rev. 126, 1962 (1962).

[26]E. R. Bernstein, J. Chem. Phys. 50, 4842 (1969).

[27](a) B. Weinstock and J. G. Malm, J. Inorg. Nucl. Chem. 2, 380 (1956); (b) J. G. Malm (private communication).

[28]J. G. Malm and H. Selig, J. Inorg. Nucl. Chem. 20, 189 (1961).

[29](a) HBr: D. H. Rank, U. Fink, and T. A. Wiggins, J. Mol. Spectrosc. 18, 170 (1965); (b) HCl: D. H. Rank, B. S. Rao, and T. A. Wiggins, J. Mol. Spectrosc. 17, 122 (1965); D. U. Webb and K. N. Rao, J. Mol. Spectrosc. 28, 121 (1968); (c) H$_2$O: E. R. Plyler and E. D. Tidwell, Mem. Soc. R. Sci.

Liege 18, 426 (1957); and L. A. Pugh and K. N. Rao, J. Mol. Spectrosc. 47, 403 (1973).

[30]See, for example, F. J. DiSalvo et al., J. Chem. Phys. 62, 2575 (1975) and reference therein.

[31]B. Weinstock, E. F. Westrum, Jr., and G. L. Goodman, Proc. Int. Conf. Low Temp. Phys., London, 1962 (1963), p. 405.

[32]J. C. Bonner and M. E. Fisher, Phys. Rev. Sect. A 135, 640 (1964).